Title: Catalase Activity is Critical for *Proteus mirabilis* Biofilm Development, EPS Composition, and Dissemination During Catheter-Associated Urinary Tract Infection

Running title: Contribution of catalase to biofilm development

Ashley N. White[1], Brian S. Learman[1], Aimee L. Brauer[1], Chelsie E. Armbruster[1#]

[1]Department of Microbiology and Immunology, Jacobs School of Medicine and Biomedical Sciences, State University of New York at Buffalo

#Correspondence:

Chelsie Elizabeth Armbruster
955 Main Street
Room 5218
Buffalo, NY 14203
(716) 829-6059
chelsiea@buffalo.edu

The authors have declared that no conflict of interest exists.

Abstract

Proteus mirabilis is a leading uropathogen of catheter-associated urinary tract infections (CAUTIs), which are among the most common healthcare-associated infections worldwide. A key factor that contributes to *P. mirabilis* pathogenesis and persistence during CAUTI is the formation of catheter biofilms, which provide increased resistance to antibiotic treatment and host defense mechanisms. Another factor that is important for bacterial persistence during CAUTI is the ability to resist reactive oxygen species (ROS), such as through the action of the catalase enzyme. Potent catalase activity is one of the defining biochemical characteristics of *P. mirabilis,* and its single catalase gene (*katA*) was recently identified as a candidate fitness factor for UTI, CAUTI, and bacteremia. Here we show that disruption of *katA* results in increased ROS levels, increased sensitivity to peroxide, and decreased biofilm biomass. The biomass defect was due to a decrease in extracellular polymeric substances (EPS) production by the Δ*katA* mutant, and specifically due to reduced carbohydrate content. Importantly, the biofilm defect resulted in decreased antibiotic resistance *in vitro* and a colonization defect during experimental CAUTI. The Δ*katA* mutant also exhibited decreased fitness in a bacteremia model, supporting a dual role for catalase in *P. mirabilis* biofilm development and immune evasion.

Introduction

Proteus mirabilis is a Gram-negative bacterium that is present in numerous environments such as soil, water, and the intestinal tracts of both humans and animals (1). However, *P. mirabilis* is also a leading uropathogen of catheter-associated urinary tract infections (CAUTIs), which are one the most common healthcare-associated infections worldwide (2-4). CAUTIs account for up to 80% of all nosocomial UTIs, and *P. mirabilis* CAUTIs are often complicated by bladder and kidney stone formation (urolithiasis), permanent renal damage, and progression to life-threatening bacteremia and sepsis (5-8). For instance, *P. mirabilis* is responsible for 12-31% of bacteremias in nursing home residents and is associated with a one-year mortality rate ranging from 10 to 66% (9-13).

P. mirabilis CAUTIs have proven difficult to treat in part due to their increasing antibiotic resistance, as well as resistant biofilm formation on the catheter surface (14-17). *P. mirabilis* is particularly well adapted for biofilm formation, causing the encrustation and blockage of urethral catheters by the formation of crystalline biofilm structures (6, 18-22). Notably, biofilms containing *P. mirabilis* have been detected on catheters even after antibiotic treatment (23-25). As *P. mirabilis* biofilms play a significant role in both the pathogenesis and treatment of CAUTI (4, 6, 26, 27), it is critical to investigate factors that influence biofilm development and antibiotic resistance in this species.

Biofilm formation is a multistep process, involving irreversible microbial attachment to a substrate, development of microcolonies, the production of extracellular polymeric substances (EPS), maturation, and dispersal, which is thought to contribute to

63 persistent infection during CAUTI and dissemination to the bloodstream (6, 28). The
64 EPS matrix is highly hydrated (98% water) and largely comprised of proteins,
65 carbohydrates, and extracellular DNA (eDNA); however, composition varies depending
66 on bacterial strain, environmental conditions, and maturation stage of the biofilm (29).
67 EPS is considered to be a critical component of bacterial biofilms, as it defines the
68 biofilm structure and is essential for the overall integrity and function of the biofilm (19,
69 28, 30).

70 The EPS matrix also plays a substantial role in the increased antimicrobial
71 resistance exhibited by bacterial biofilms (17). There are several ways in which biofilm
72 formation impacts antimicrobial susceptibility. First, the antimicrobial agents must
73 diffuse through the EPS matrix in order to act on the organisms within the biofilm. The
74 EPS effectively acts as a shield that prevents diffusion of antimicrobials either by
75 binding and chemically inhibiting the antimicrobial molecules or by limiting their rate of
76 infiltration (31, 32). The biofilm-associated bacteria also experience reduced growth
77 rates and are less metabolically active, which limits the efficacy of many antimicrobial
78 agents (33). Lastly, the environment that immediately surrounds the biofilm may provide
79 conditions that further protect the biofilm-associated bacteria (33). As a result, biofilm
80 formation on indwelling medical devices poses a serious challenge due to the increased
81 resistance of biofilm-associated organisms to antimicrobial agents (28).

82 Another factor that contributes to bacterial persistence and pathogenicity is the
83 ability to resist reactive oxygen species (ROS) (34). For instance, many bacterial
84 species produce a catalase enzyme, which reduces hydrogen peroxide (H_2O_2) to water
85 (H_2O) and oxygen (O_2), and has been shown to protect biofilm associated

Pseudomonas aeruginosa by preventing full penetration of H_2O_2 through the biofilm matrix (34). Hydrogen peroxide is the longest-lived reactive oxygen species, and it can cause critical damage to both the bacterial cell membrane and essential cellular macromolecules such as proteins, lipids, and nucleic acids (35, 36). ROS can also contribute to the effectiveness of antibiotic mediated killing. For example, antibiotic exposure induces oxidative stress in *P. aeruginosa,* and antibiotic susceptibility was increased by disruption of a gene involved in reducing H_2O_2 (*ahpC*), indicating that ROS generation contributed to drug lethality (37). It has therefore been proposed that interfering with bacterial protection against ROS could improve antibiotic treatment, even for biofilms (37-40).

Potent catalase activity is one of the defining biochemical characteristics of *P. mirabilis* (41), and there are several indications that the single catalase gene (*katA*) of *P. mirabilis* is important for both fitness and pathogenicity during infection. For instance, *katA* was found to be upregulated during infection in a mouse model of UTI (42), it was identified as a candidate fitness factor during both single-species and polymicrobial CAUTI (43), and it was detected as an infection-specific fitness factor for survival in the bloodstream (44). Despite this evidence, the exact role of catalase in *P. mirabilis* pathogenesis had yet to be experimentally validated. In this study, we disrupted the *katA* gene in *P. mirabilis* strain HI4320 and investigated the contribution of catalase to bacterial growth, motility, ROS tolerance, biofilm formation, antibiotic resistance, pathogenicity within the urinary tract, and fitness within the bloodstream. We show that loss of *P. mirabilis* catalase activity does not alter *in vitro* growth or planktonic antibiotic susceptibility, but peroxide detoxification is critical for production of a mature biofilm.

The absence of catalase severely alters the composition of the EPS matrix, resulting in increased antibiotic susceptibility of biofilm-associated bacteria. Additionally, we demonstrate that catalase contributes to the pathogenesis of *P. mirabilis* during CAUTI and fitness during bacteremia.

Results

Generation and characterization of a P. mirabilis ΔkatA mutant

In order to investigate the importance of catalase activity to *P. mirabilis* growth, biofilm formation, and pathogenesis, a mutant was generated in *P. mirabilis* strain HI4320 to disrupt the catalase gene (*katA*) by insertion of a kanamycin resistance cassette. Disruption of the *katA* gene and resulting catalase activity were confirmed by PCR and a catalase foam height assay (Fig. 1A). As expected, the Δ*katA* mutant was catalase-negative when exposed to hydrogen peroxide, and providing the *katA* gene on a plasmid restored catalase activity. The complemented activity was more potent than that of the parental strain, which is likely due to plasmid copy number. The Δ*katA* mutant grew similarly to wild-type *P. mirabilis* in LB broth and did not exhibit any defects in swimming motility, swarming motility, or urease activity (Fig. 1B-E), indicating that disruption of the *katA* gene does not affect standard laboratory behaviors of *P. mirabilis*. Disruption of *katA* also had no impact on expression of either adjacent gene by qRT-PCR (Fig. S1). Taken together, these data indicate that targeted disruption of *katA* abrogates catalase activity without obvious polar effects.

Disrupting katA increases sensitivity to hydrogen peroxide and steady-state ROS levels

In order to define the limits of hydrogen peroxide each strain could withstand, we conducted a hydrogen peroxide sensitivity growth curve wherein each strain was cultured in LB broth with increasing concentrations of H_2O_2. The Δ*katA* mutant was susceptible to ~2 mM H_2O_2 and completely inhibited by ~3 mM (Fig. 2B, C). In contrast,

~109 mM H_2O_2 was needed to impair growth of wild-type *P. mirabilis* and ~326 mM H_2O_2 for complete growth inhibition (Fig. 2D, E). Importantly, providing the *katA* gene on a plasmid allowed the Δ*katA* mutant to tolerate higher H_2O_2 concentrations than the wild-type strain (Fig. 2E), again likely due to a high plasmid copy number.

A luminescence-based H_2O_2 assay was next used to determine the extent of H_2O_2 accumulation in wild-type *P. mirabilis* and the Δ*katA* mutant during growth in broth culture to gauge the contribution of catalase activity to detoxification of endogenously-produced ROS. For these experiments, a standard curve was generated by supplementing Δ*katA* cultures with increasing concentrations of peroxide at the time of ROS measurement (Fig. 2F). After 4 hours of culture in LB broth, samples from wild-type *P. mirabilis* contained an average of 109 ± 26.9 μM H_2O_2, while the Δ*katA* samples contained an average of 135 ± 39.7 μM H_2O_2 (1.24 fold greater than wild-type, Fig. 2G, H). Notably, the concentration of H_2O_2 in the Δ*katA* samples is ~15-fold lower than the concentration at which growth of Δ*katA* was perturbed (~2mM, as seen in Fig.2B), suggesting that the loss of catalase activity likely does not induce a significant state of oxidative stress during growth in LB broth. However, it could cause the Δ*katA* mutant to be more susceptible to additional ROS insult or other stressors.

The ΔkatA mutant exhibits a defect in biofilm development

As biofilm formation is a critical component of *P. mirabilis* pathogenesis during CAUTI, we next assessed biofilm formation by the Δ*katA* mutant at 2, 4, 6, 12, and 20 hours (Fig 3). By crystal violet staining, wild-type *P. mirabilis* established a robust biofilm over the 20 hour incubation in LB broth, but the Δ*katA* mutant exhibited a significant

159 decrease in total biomass that was detectable at 4 hours and remained evident for the
160 rest of the time course (Fig. 3A). Importantly, assessment of viable bacteria within the
161 biofilms at each time point revealed that the defect was not due to a decrease in
162 bacterial CFUs, and therefore likely represents a defect in biofilm architecture (Fig. S2).
163 These results were also recapitulated for biofilms established in pooled human urine, as
164 a physiologically-relevant growth medium for CAUTI (Fig. 3B).

165 To define the specific contribution of peroxide detoxification to *P. mirabilis* biofilm
166 formation, wild-type *P. mirabilis* and the *ΔkatA* mutant were supplemented with an
167 amount of bovine catalase that results in the equivalent foam height produced by $1x10^8$
168 CFU/ml of wild-type *P. mirabilis* (~0.7 mg , ~40,000 units). The addition of bovine
169 catalase had no impact on biofilm development by wild-type *P. mirabilis* in LB, but fully
170 restored biofilm biomass for the *ΔkatA* mutant in both LB and human urine, albeit not
171 until the 20 hour time point (Fig. 3A, B). These data suggest that catalase is important
172 for later stages of biofilm development and maturation rather than the initial stages of
173 attachment and microcolony formation. Importantly, the contribution of bovine catalase
174 was confirmed to specifically derive from enzymatic activity, as both 10 kDa filtration
175 and heat inactivation of the catalase solution abrogated complementation of the *ΔkatA*
176 mutant biofilm defect (Fig. S3).

177 To verify that the contribution of catalase to *P. mirabilis* biofilm development
178 pertains specifically to peroxide detoxification, we next sought to determine if the
179 addition of a non-lethal concentration of peroxide (~109 mM, as seen in Fig. 2D) could
180 impair biofilm formation by wild-type *P. mirabilis*. The addition of peroxide at the time of
181 inoculation significantly decreased the *P. mirabilis* biofilm biomass for the first 6 hours of

biofilm development, after which time enough of the peroxide was likely broken down to restore full biofilm development (Fig. 3C). Similar results were also recapitulated in pooled human urine (Fig. 3D). Taken together, these data confirm that the biofilm defect of the *ΔkatA* mutant is specifically due to the loss of catalase activity and peroxide detoxification, and likely pertains to biofilm maturation.

We next sought to determine if the biofilm defect of the *ΔkatA* mutant may be the result of increased oxidative stress. Throughout the time course of biofilm development, samples were taken from the *ΔkatA* mutant and wild-type *P. mirabilis* to examine the relative expression level of two additional peroxide detoxifying enzymes (alkylhydroperoxidases *ahpC* PMI1213 and PMI0073) and three superoxide dismutases (*sodA*, *sodB*, *sodC)*. Expression of each gene was normalized to *rpoA,* and relative expression over time was determined for the wild-type strain alone and the *ΔkatA* mutant in comparison to the wild-type (Fig S4). Expression of genes involved in peroxide detoxification (*katA*, PMI1213 and PMI0073) remained unaffected in the wild-type strain over the time course of biofilm development (Fig. S4A-C); however, expression of genes involved in superoxide detoxification (*sodA*, *sodB*, and *sodC*) were significantly upregulated over time (Fig. S4D-F). This suggests that wild-type *P. mirabilis* experiences some degree of oxidative stress during biofilm formation, and is primarily due to superoxide. If disruption of catalase and resulting accumulation of endogenous peroxide generated substantial oxidative stress, we would expect to see increased expression of some or all of these genes in the *ΔkatA* mutant relative to wild-type *P. mirabilis*. However, none of the selected genes exhibited a significantly different expression pattern in Δ*katA* biofilms in comparison to the wild-type biofilms (Fig. S4H-

L). Thus, while *P. mirabilis* does exhibit signs of oxidative stress during biofilm formation, loss of catalase activity does not cause a substantial increase in oxidative stress.

Δ*katA exhibits a defect in biofilm EPS composition*

Since the *ΔkatA* mutant exhibited a defect in biofilm biomass independent of cell viability or oxidative stress, these data led us to investigate the overall composition of the biofilm. Aside from bacterial aggregates, the other major component of bacterial biofilms is the matrix of extracellular polymeric substances (EPS) that coats and protects the bacterial cells from the surrounding environment. To qualitatively assess biofilm composition, we utilized scanning electron microscopy (SEM). Biofilms formed by wild-type *P. mirabilis* for 20 hours were heavily coated with EPS (Fig. 4A), while biofilms formed by the Δ*katA* mutant displayed a similar degree of aggregated clusters of bacteria but were lacking the extensive EPS coating of the wild-type biofilms (Fig. 4B). Importantly, the addition of bovine catalase at the time of inoculation slightly enhanced EPS production by wild-type *P. mirabilis* (Fig 4C) and fully restored EPS production by the Δ*katA* mutant (Fig 4D). These data indicate that the biomass defect of the Δ*katA* mutant is likely due to a decrease in the production of EPS.

The exact composition of *P. mirabilis* HI4320 biofilm EPS has not been fully elucidated in the literature; however, the EPS of bacterial biofilms is generally comprised of proteins, carbohydrates, and extracellular DNA (eDNA). To assess biofilm EPS composition, wild-type *P. mirabilis* and the Δ*katA* mutant were incubated for 20 hours in LB broth with aeration (planktonic suspension, PS) or stationary in wells of a

24-well plate from which a total biofilm sample was collected (biofilm suspension, BS). The remaining biofilm material was then treated with formaldehyde to fix the bacterial cells and prevent lysis during subsequent steps of EPS extraction, and NaOH to promote dissociation of the EPS from the biofilm and increase its solubility. Following these treatments, a cellular fraction (CF) and dialyzed EPS fraction (EF) were collected. No differences in eDNA concentration were observed between strains in any of the tested fractions (Fig. 4E), and total protein measurement revealed only a slight decrease in the Δ*katA* biofilm suspension compared to wild-type (Fig. 4F). However, total carbohydrate measurement revealed a substantial decrease in the biofilm suspension and EPS fraction of the Δ*katA* mutant compared to wild-type *P. mirabilis* (Fig. 4G). Thus, the biofilm biomass defect of the Δ*katA* mutant derives from a decrease in EPS carbohydrate content.

Δ*katA biofilms exhibit increased antibiotic susceptibility*

Due to the enhanced antimicrobial resistance of bacteria in a biofilm mode of growth, we sought to determine the impact of the Δ*katA* biofilm biomass defect on antibiotic susceptibility. Wild-type *P. mirabilis* and the Δ*katA* mutant were treated with two antibiotics that target the bacterial cell wall (ampicillin and ceftriaxone) and one that targets DNA replication (ciprofloxacin) during planktonic growth or after 20 hours of biofilm growth. The Δ*katA* mutant did not exhibit substantial differences in susceptibility to ampicillin or ciprofloxacin during planktonic growth, although a slight decrease was detected for ceftriaxone at 0.02 and 0.01 µg/ml (Fig. 5A-C). However, Δ*katA* 20 h biofilms were more susceptible to all three antibiotics, suggesting that the decrease in

biofilm biomass impacts antibiotic susceptibility (Fig. 5D-F). To further explore the importance of the biofilm defect for antibiotic susceptibility, biofilms formed by wild-type and the Δ*katA* mutant were also treated after only 4 hours of development, as this was the earliest time point corresponding to a significant decrease in biofilm biomass for the Δ*katA* mutant. Earlier exposure to antibiotics resulted in greater killing of both strains and further magnified the defect of the Δ*katA* mutant (Fig. 5G-I). Importantly, the addition of bovine catalase restored the antibiotic resistance of the Δ*katA* mutant biofilms to an equivalent or even greater level than the wild-type strain (Fig. 5G-I). Thus, we conclude that loss of *katA* results in a biofilm-specific increase in antibiotic susceptibility due to disruption of EPS production and biofilm maturation.

The biofilm biomass defect of the ΔkatA mutant can be recapitulated on Foley catheters

The bacterial biofilms that drive persistent infection in CAUTI are most often formed on the surface and within the lumen of the catheters themselves. We therefore sought to determine if the Δ*katA* biofilm biomass defect is similarly present when biofilms are formed directly on a silicone Foley catheter. Sterile Foley catheters (size 14 French) were cut into 15-mm segments, suspended in the wells of a 24 well plate, and inoculated with either wild-type *P. mirabilis* or the Δ*katA* mutant in LB broth. Biofilms were established for 20 hours, after which time the catheter segments were removed, air dried, and biofilm biomass was measured using an optimized crystal violet assay. Wild-type *P. mirabilis* established robust biofilms on the silicone catheter segments, and the Δ*katA* mutant again exhibited a substantial biomass defect that could be

274 complemented by the addition of bovine catalase at the time of inoculation (Fig. 6A, B).
275 Thus, the Δ*katA* biofilm biomass defect is present on a physiologically-relevant biofilm
276 substrate for CAUTI.

277

278 ***Catalase contributes to both pathogenesis and fitness in vivo***

279 Considering the important contribution of bacterial biofilms to CAUTI in humans,
280 we next sought to determine the contribution of *P. mirabilis* catalase to colonization and
281 pathogenicity during experimental CAUTI. To test this, we utilized a mouse model of
282 CAUTI as previously described (45). Briefly, female CBA/J mice were transurethrally
283 inoculated with 1 x 10^5 CFU of either wild-type *P. mirabilis* or the Δ*katA* mutant, and a 4-
284 mm segment of sterile silicone catheter tubing was inserted into the bladder at the time
285 of inoculation to recapitulate CAUTI. Weight loss was monitored daily (Fig. S5) and
286 mice were euthanized at 24 or 96 hours post inoculation (hpi) to quantify bacterial
287 burden in urine, bladder, and kidneys, as well as the spleen as an indication of
288 bacteremia. Infection with wild-type *P. mirabilis* resulted in slightly greater weight loss at
289 24 hpi than infection with the Δ*katA* mutant, but no significant differences were detected
290 at later time points (Fig. S5A). Similar colonization levels were observed between
291 strains in the urine, bladder, and kidneys at 24 hpi. However, the Δ*katA* mutant
292 exhibited reduced spleen colonization at this time point (Fig. 7A), which could indicate a
293 defect either in dissemination from the urinary tract to the bloodstream or decreased
294 survival once within the bloodstream. Mice from both infection groups exhibited
295 increased bacterial burden and disease severity at 96 hpi compared to 24 hpi, although
296 there were no significant differences between infection groups at this time point (Fig. 7B

297 and Table 1). Thus, while the Δ*katA* mutant exhibited reduced spleen CFUs at 24 hpi,
298 pathogenesis was equivalent to wild-type by 96 hpi.

299 A caveat to the CAUTI model is that the bacterial inoculum is introduced as a
300 suspension, and biofilm formation occurs concurrently with defense against the host
301 immune response. In order to isolate the contribution of the Δ*katA* biofilm defect to *P.*
302 *mirabilis* pathogenesis during CAUTI, we next inoculated mice with catheter segments
303 that had been pre-colonized for 12 hours by either wild-type *P. mirabilis* or the *ΔkatA*
304 mutant to establish catheter biofilms. Importantly, pre-colonizing the catheter segments
305 for 12 hours resulted in a similar inoculum as injection of a bacterial suspension (~1 x
306 10^5 CFU) but caused a more robust infection with pronounced weight loss and disease
307 severity after just 24 hpi (Fig. S5B and Table 1C), such that the experiment could not be
308 extended past this time point. Mice infected with wild-type *P. mirabilis* pre-colonized
309 catheters exhibited more uniform urine and bladder CFUs than in the traditional CAUTI
310 model (Fig. 7C vs 7A), as well as a significantly higher incidence of hematuria and
311 hematoma, kidney discoloration and mottling, and macroscopically-visible kidney stones
312 (Table 1). Infection with the Δ*katA* mutant also displayed greater uniformity in urine and
313 bladder CFUs in the pre-colonized model compared to the traditional CAUTI model;
314 however, in comparison to wild-type *P. mirabilis,* the Δ*katA* mutant exhibited a profound
315 decrease in kidney colonization and a significantly lower incidence of hematuria,
316 bladder hematoma, and kidney stones, as well as a trend towards reduced bacterial
317 burden in the urine and spleen (Fig. 7C and Table 1). Based on these data, wild-type
318 displays greater infection severity and the Δ*katA* mutant displays a more pronounced
319 defect when the infection is seeded from a pre-colonized catheter, which underscores

320 the importance of *P. mirabilis* biofilm development and EPS composition for CAUTI
321 pathogenesis.

322 While the pre-colonized catheter model clearly demonstrates a pathogenesis
323 contribution for catalase stemming from its role in biofilm development, these studies
324 cannot exclude a role for catalase in defense against ROS. Neutrophils are the first and
325 most abundant immune cells recruited to the bladder in response to CAUTI, and
326 neutrophil oxidative burst represents a robust source of ROS (46-48). Neutrophils
327 appear to be the major factor that limits bacterial growth in the urinary tract during the
328 initial 24 hours post infection (49), and many of the defense strategies used by
329 neutrophils rely on oxidative mechanisms involving ROS (48, 50, 51). The oxidative
330 burst of a single neutrophil has been shown to generate 1–10 μM hydrogen peroxide,
331 and neutrophils in suspension (~10^6/ml) are capable of producing steady-state
332 concentrations of ~10 μM (46). Thus, the decreased kidney and spleen CFUs for the
333 Δ*katA* mutant support an additional role for catalase in protection against host defenses
334 during dissemination and possibly survival within the bloodstream, in which biofilm
335 formation is not likely to play a role.

336 To investigate biofilm-independent fitness of the Δ*katA* mutant, mice were
337 inoculated via tail vein injection of a 1:1 mixture of wild-type *P. mirabilis* and Δ*katA*. All
338 mice exhibited high bacterial burden in the spleen, liver, and kidneys 24 hpi (Fig. 7D),
339 and the Δ*katA* mutant was significantly outcompeted by wild-type *P. mirabilis* in the liver
340 and kidneys indicating a biofilm-independent fitness defect (Fig. 7E). As neutrophil
341 oxidative burst represents a potent source of hydrogen peroxide during CAUTI, we next
342 investigated the contribution of *P. mirabilis* catalase to defense against

343 opsonophagocytic killing by neutrophils. Interestingly, the Δ*katA* mutant was no more
344 susceptible to opsonophagocytic killing than wild-type *P. mirabilis* (Fig. S6). These data
345 indicate that the contribution of catalase to fitness within the bloodstream is likely due to
346 factors other than defense against neutrophil oxidative burst.

Discussion

The high degree of resistance against antimicrobials and host defenses that is conferred by bacterial biofilms represents a substantial challenge for the effective treatment of medical device-related infections, including CAUTI. Catheter biofilms containing *P. mirabilis* pose an additional challenge as they are typically comprised of bacterial aggregates, EPS, and crystalline deposits as a result of urease activity, and these crystalline biofilms can result in complete obstruction of urine flow (6). In general, *P. mirabilis* clinical isolates also exhibit a high degree of antimicrobial resistance, including intrinsic tolerance to tetracycline and polymyxin class drugs, acquisition of resistance to aminoglycosides and fluoroquinolones, and the spread of extended-spectrum beta-lactamases and carbapenemases (52-55). Combined with the added resistance provided by the biofilm mode of growth, these properties collectively contribute to the high mortality rate for *P. mirabilis* CAUTI and bacteremia (56-60). Investigation of the processes that contribute to *P. mirabilis* biofilm development and antimicrobial resistance are therefore critical to uncover new potential targets for prevention and treatment.

P. mirabilis has long been characterized as having potent catalase activity, and its single catalase gene (*katA*) has been implicated as contributing to infection in three prior genome-wide screens: 1) *katA* expression was upregulated during infection in a mouse model of UTI (42); 2) *katA* was identified as a candidate fitness factor during both single-species and polymicrobial CAUTI (43); and 3) *katA* was detected as an infection-specific fitness factor for survival in the bloodstream (44). We therefore endeavored to delineate the contribution of catalase to several stages of *P. mirabilis*

pathogenesis. Here, we show that disruption of catalase results in a slight increase in ROS levels during growth in broth culture, which does not appear to induce oxidative stress in *P. mirabilis* but does increase sensitivity to additional peroxide insult. We also uncovered a critical role for peroxide detoxification via catalase activity in the production of a mature biofilm by *P. mirabilis.* Specifically, loss of catalase activity decreased biofilm biomass due to a severe alteration of EPS composition, particularly the carbohydrate fraction. Importantly, this EPS defect rendered the Δ*katA* biofilms more susceptible to antibiotics and also decreased colonization and dissemination in a mouse model of CAUTI.

The exact sugar moieties that comprise the EPS of *P. mirabilis* strain HI4320 have yet to be fully elucidated; however, hexose moieties previously identified in the LPS outer core of *P. mirabilis* (glucose, galactose, and N-acetyl glucosamine) are likely involved (61, 62). Further exploration is needed to identify the specific carbohydrate moieties that are decreased in the Δ*katA* mutant, and to pinpoint the steps at which loss of catalase activity impacts carbohydrate biosynthesis and EPS production. Regardless, the decrease in EPS-associated carbohydrates clearly resulted in increased antibiotic susceptibility of the Δ*katA* biofilm. EPS defects have been demonstrated to impact biofilm formation and antibiotic susceptibility of other Gram-negative bacteria. For instance, *katA* is important for *P. aeruginosa* biofilm development and biofilm-dependent resistance of treatment with high concentrations of H_2O_2 (63), and biofilms formed by *P. aeruginosa* Δ*psl* (polysaccharide synthesis locus) mutants exhibit increased antibiotic susceptibility (64, 65). Our data also fit within existing literature that have revealed a contribution of catalase to biofilm architecture (66). In *Mycoplasma pneumoniae* (an

organism that lacks superoxide dismutase and catalase), treatment with catalase enhanced biofilm formation and altered biofilm structure, such that fewer and smaller tower structures were produced and the resulting biofilms were smoother and more homogenous (3). While treatment of wild-type *P. mirabilis* with bovine catalase did not impact total biofilm biomass, our electron microscopy images suggest that it may increase EPS production and biofilm smoothness. Full determination of *P. mirabilis* HI4320 EPS carbohydrate composition will be necessary to reveal which components are altered when catalase is disrupted, and which (if any) are increased in the wild-type strain upon supplementation with excess catalase.

We also revealed that disruption of *P. mirabilis* catalase results in a biofilm-dependent defect in a mouse model of CAUTI and a biofilm-independent defect in fitness within the bloodstream, thereby demonstrating two separate contributions of the *P. mirabilis* catalase enzyme to pathogenesis. Pre-colonizing the catheter resulted in greater overall bacterial colonization during CAUTI than delivery of a bacterial suspension, which highlights the importance of biofilm formation in CAUTI pathogenesis. The pre-colonized catheter also resulted in greater infection severity overall, as seen by the increased incidence of hematuria and hematoma, kidney discoloration and mottling, and macroscopically-visible kidney stones. These results are in agreement with other investigations concerning the pathogenic potential of biofilm-associated bacteria and bacterial populations that are newly dispersed from a biofilm (66). For instance, *Streptococcus pneumoniae* that have been dispersed from a biofilm have distinct phenotypic properties that differ from those of either biofilm-associated or

415 broth-grown planktonic bacteria, including differential gene expression and increased
416 ability to disseminate and cause infection (67).

417 The colonization defect of the Δ*katA* mutant that was observed in the spleen
418 during both CAUTI models is also notable, as it could indicate a reduced capacity of the
419 mutant to disseminate from the urinary tract to the spleen, a defect in resistance against
420 host defenses and survival within the bloodstream, or a combination thereof. Since the
421 Δ*katA* mutant also exhibited a fitness defect during direct competition with the wild-type
422 strain in a bloodstream infection, the spleen colonization defect likely pertains to a
423 reduced capacity to survive host immune defenses, such as neutrophil oxidative burst.
424 However, the Δ*katA* mutant was no more susceptible to neutrophil opsonophagocytic
425 killing than the parental strain. One possible explanation for this observation is that
426 neutrophil-mediated killing of *P. mirabilis* may be largely due to non-oxidative
427 mechanisms, such as granule fusion rather than oxidative burst (68-70). Alternatively,
428 *P. mirabilis* catalase may be more critical for resistance of oxidative burst from other cell
429 types, such as macrophages (71, 72). A third possibility is that the slight increase in
430 peroxide levels that occurs in the Δ*katA* mutant may render it more sensitive to other
431 non-oxidative host defenses. Further exploration will be necessary to fully elucidate the
432 role of *P. mirabilis* catalase in immune evasion.

433 In summary, peroxide detoxification via catalase activity is a critical component of
434 *P. mirabilis* pathogenesis due to a role in biofilm development, antimicrobial resistance,
435 and resistance of host defenses. Elucidation of the underlying mechanism through
436 which catalase impacts carbohydrate and EPS production may uncover new strategies
437 for preventing *P. mirabilis* biofilm formation, disrupting existing biofilms, or increasing

438 sensitivity to ROS and antimicrobial agents. Such strategies could be particularly
439 beneficial for patient populations requiring long-term catheterization.

Materials and Methods

Ethics Statement. All animal protocols were approved by the Institutional Animal Care and Use Committee (IACUC) at the State University of New York at Buffalo, Jacobs School of Medicine and Biomedical Sciences (MIC31107Y), and were in accordance with the Office of Laboratory Animal Welfare (OLAW), the United States Department of Agriculture (USDA), and the guidelines specified by the Association for Assessment and Accreditation of Laboratory Animal Care, International (AAALAC, Intl.).

Bacterial Strains and Culture Conditions. *Proteus mirabilis* strain HI4320 was previously isolated from the urine of a catheterized patient (73). The *P. mirabilis* Δ*katA* mutant was constructed in strain HI4320 by the insertion of a kanamycin resistance cassette into the *katA* gene according to the Sigma TargeTron group II intron protocol, as previously described (74). Mutants were verified by selection on kanamycin, PCR, and catalase foam height assay (see below). As insertion of a kanamycin cassette via TargeTron retrohoming can result in polar effects, the Δ*katA* mutant was complemented by PCR-amplifying the wild type *katA* gene and 500 bp of flanking sequences, ligating into a linearized pGEN-MCS vector, electroporation, and selection on ampicillin. Primers used for the generation of the Δ*katA* mutant and Δ*katA*+ complement are provided in Supplementary Table 1. *P. mirabilis* HI4320 (wild-type) and the Δ*katA* mutant were routinely cultured at 37°C with aeration in 5 mL of LB broth (10 g/L tryptone, 5 g/L yeast extract, 0.5 g/L NaCl) or on Low salt LB agar (10 g/L tryptone, 5 g/L yeast extract, 0.1

462 g/L NaCl, 15 g/L agar). Biofilm assays were performed using LB broth (10 g/L tryptone,
463 5 g/L yeast extract, 0.5 g/L NaCl) or filter-sterilized human urine (Cone Bioproducts,
464 Sequin, TX).

465

466 **Catalase Foam Height Assay.** 100 µl of an overnight culture of each strain was added
467 to a 12 x 75 mm polystyrene tube. Subsequently, 100 µl of 1% Triton X-100 and 100 µL
468 of 30% v/v hydrogen peroxide were added to the tubes, mixed thoroughly, and
469 incubated at room temperature for ~5 minutes. Following completion of the reaction, the
470 height of O2-forming foam in the test tube was observed.

471

472 **Growth Curves.** Bacterial overnight cultures were diluted 1:100 into fresh LB and
473 grown in 96-well plates at 37°C with aeration via double orbital shaking in a BioTek
474 Synergy H1. Growth was assessed by measurement of OD_{600} at 15-minute intervals for
475 18 hours. For hydrogen peroxide sensitivity growth curves, indicated concentrations of
476 hydrogen peroxide were added to the media at the time of inoculation.

477

478 **Urease Assay.** Urease activity was measured as described previously (45). Briefly,
479 overnight cultures of bacteria were washed once in sterile saline and adjusted to ~5 ×
480 10^9 CFU/ml. Cultures were then diluted 1:10 in filter-sterilized human urine
481 supplemented with 0.001% wt/vol phenol red and 500 mM urea and dispensed into the
482 wells of a clear-bottom 96-well plate. Absorbance (OD_{562}) was measured every 30 sec
483 for a total of 90 min in a BioTek Synergy H1.

Motility Assays. Swimming motility agar plates (MOT; 10 g/L tryptone, 0.5 g/L NaCl, 3 g/L agar) were stab inoculated with an overnight culture of wild-type *P. mirabilis* or Δ*katA* mutant and incubated without inverting at 30°C for 16 h prior to the measurement of swimming diameter. Swarming was assessed by inoculating 5 µl of an overnight culture of wild-type *P. mirabilis* or Δ*katA* mutant onto the surface of a swarm plate (LB agar with 5 g/L NaCl), allowing the inoculum to soak in for ~10 min, and incubating at 37°C for 16 h prior to the measurement of the diameter of each swarm ring.

ROS Quantification. The ROS-Glo™ H_2O_2 Assay Kit (Promega™) was used per the manufacturer's specifications, with the following modifications to measure the basal level of H_2O_2 present in the wild-type and Δ*katA* mutant strain in broth culture. Overnight cultures of each strain were centrifuged, washed once with fresh LB, adjusted to the same optical density, diluted 1:100 in fresh LB, and incubated at 37°C with aeration for 4 hours. After the 4 hour incubation, 80 µl of each sample was added to a 96 well plate with 20 µl of derivatized luciferin substrate and incubated for 30 min at 37°C. To generate a standard curve, a series of Δ*katA* samples were supplemented with increasing concentrations of H_2O_2 or an equivalent volume of distilled H_20. 100 µl of ROS-Glo™ detection solution was then added to each well, incubated at room temperature for 20 min, and the relative luminescence units (RLU) were read in a BioTek Synergy H1.

Biofilm Formation for Determination of Viability. Static biofilm formation was performed in tissue culture treated 24-well plates (Falcon 353047) by introducing ~2 x 10^7 CFU/ml of either wild-type *P. mirabilis* or the Δ*katA* mutant into 1.5 mL LB broth per well and incubating at 37°C for 20 h. Blank wells for normalization contained only assay medium (LB broth or urine). Following incubation, supernatants were removed and biofilms were washed twice with 1x PBS to remove any remaining planktonic bacteria. A volume of 1.5 mL of sterile PBS was then added to each well and biofilms were scraped with a sterile micropipette tip to resuspend viable bacteria contained within each biofilm. Samples underwent serial 10x dilutions and were spiral plated (Eddy Jet 2, Neutec Group inc, Farmingdale, NY) onto low salt LB agar for enumeration of CFU using a ProtoCOL 3 automated colony counter (Synbiosis).

Biofilm Biomass Analysis. 20 h biofilm formation was performed as above. Where indicated, biofilms were supplemented at time of inoculation with either 0.7 mg of active bovine catalase liver enzyme (~40,000 units) or 0.1% v/v (~109 mM) of H_2O_2. Supernatants were then carefully removed from wells of a 24-well plate using a VIAFLO Voyager automated pipette (Integra Biosciences, Hudson, NJ), inserted slowly at a 45° angle while making sure to avoid touching the sides and bottom of wells, and set to a speed of 2 for gentle aspiration. Biofilms were air dried for 5 min, stained with 1.5 mL 0.1% crystal violet for 10 min, washed once with distilled H_2O to remove excess stain, and solubilized in 2 mL of 95% ethanol for 10 min on an orbital shaker at 210 rpm. The wells of the 24-well plate containing the biofilms were then scraped and resuspended with a micropipette tip to ensure all stained biofilm material was solubilized. Crystal

violet absorbance (OD_{570}) was measured in a BioTek Synergy H1, and blanked using cell-free control wells for each biofilm assay.

Catheter Biofilm Biomass Analysis. Biofilms were established in 24-well plates as described above, and a 15 mm segment of silicone Foley catheter (Bard 57165814, size 14 French) was placed in the wells at the time of inoculation. After 20 h, catheter segments were transferred into empty wells of a new 24-well plate, all residual LB supernatant was removed from the catheter lumen, and the segments were air dried for 15 min. The segments were then stained with 1.5 mL 0.1% crystal violet for 10 min, washed by gently dunking in distilled H_2O to remove excess stain, and solubilized in a microfuge tube containing 1 mL of 95% ethanol. The tubes were then transferred to a water bath sonicator for a total of 10 minutes (vortexing every 5 minutes) to ensure removal of the biofilms from the catheter segments. Tubes were then incubated at room temperature at 220 rpm for 10 minutes to ensure full solubilization. The now-clean catheter segments were removed from the solubilized solution, solubilized solutions received a final vortex, and crystal violet absorbance (OD_{570}) was measured in a BioTek Synergy H1. Absorbance was blanked using cell-free catheters for each biofilm assay.

Antibiotic Susceptibility Assay. The following antibiotics were diluted as per manufacturer specifications and made fresh before each experiment: ampicillin sodium salt (Research Products International A40040), ceftriaxone sodium salt (Cayman Chemical 18866), and ciprofloxacin (Tokyo Chemical Industry C2510). For planktonic

551 bacteria, antibiotic susceptibility was determined by assessing growth in increasing
552 concentrations of each antibiotic via OD_{600} as above. Antibiotic susceptibility of biofilms
553 was determined by establishing biofilms as above. After either 4 h or 20 h (as indicated
554 in the text), supernatants were carefully removed and replaced with fresh LB containing
555 increasing concentrations of each antibiotic. Biofilms were then incubated for an
556 additional 20 h, and viable CFUs/mL were determined as above.

557

558 **Scanning Electron Microscopy.** Biofilms were established on 12mm circular micro
559 cover glass (VWR) within 24-well plates following the same protocol as above. The
560 supernatants were aspirated using a vacuum manifold fitted with a 300 µL tip, inserted
561 slowly at a 45° angle while making sure not to touch the coverslip. Coverslips were
562 gently transferred via sterile forceps to a new/sterile well and biofilms were fixed for 1 h
563 with 2.5% glutaraldehyde in 0.1 M sodium cacodylate buffer containing 0.075%
564 ruthenium red and 0.075 M lysine acetate, pH 7.2. Samples were rinsed three times
565 with 0.2 M sodium cacodylate buffer containing 0.075% ruthenium red (pH 7.2) and then
566 subjected to graded incubations in 30%, 50%, 75%, 95%, and 100% ethanol. Samples
567 were submerged twice in 100% hexamethyldisilazane and air dried. Scanning electron
568 microscopy (SEM) images were captured at the University at Buffalo South Campus
569 Instrument Center using a Hitachi SU-70 microscope equipped with a tilt stage for side
570 angle views.

571

572 **EPS Isolation and Analysis.** The following protocol was adapted from Bales et al. (75).
573 Biofilms were established in 24-well plates for 20 h as described above and 20 h
574 planktonic samples of each strain were also grown as above. At the 20 h time point, the
575 planktonic samples were normalized by optical density and 1 ml of each was
576 centrifuged, supernatants were removed, cell pellets were resuspended in sterile Milli-Q
577 H_2O, and the resulting planktonic suspension (PS) was aliquoted and frozen until future
578 use. Supernatants were removed from the biofilm samples, and all biofilm material from
579 the entire 24-well plate was scraped and resuspended into 3 ml sterile Milli-Q H_2O. A
580 portion of the resulting biofilm suspension (BS) was aliquoted and frozen until future
581 use, and the rest was transferred to sterile microfuge tubes and treated with 6 µl of 37%
582 formaldehyde solution per 1ml to fix the cells and prevent lysis during subsequent
583 extraction steps. The mixture was incubated at room temperature in a chemical hood
584 with gentle shaking (100 rpm) for 1 hour. 400 µl of 1 M NaOH was then added for each
585 1 ml of biofilm suspension and incubated at room temperature with gentle shaking (100
586 rpm) for 3 hours to extract EPS. Cell suspensions were then centrifuged (20,000 rcf) for
587 1 hour at 4°C. The supernatant containing soluble EPS was transferred to a new sterile
588 microfuge tube, while the cellular pellet was resuspended in 1 ml of sterile Milli-Q H_2O
589 and the resulting cellular fraction (CF) was aliquoted and frozen until future use. The
590 EPS was then filtered through a Spin-X 0.22 µm centrifuge tube filter (Costar 8160) and
591 dialyzed against sterile milli-Q H_2O (~300X's the volume of the sample) using a 3.5K
592 MWCO Slide-A-Lyzer® Dialysis Cassette (Thermo Scientific). Samples were dialyzed
593 for ~18 h at room temperature with H_2O changes at 2 and 4 hours. The resulting
594 dialyzed EPS fractions (EF) were aliquoted and frozen until future use.

595 For EPS component analyses, all isolated fractions (PS, BS, CF, and EF) were
596 thawed and analyzed for characterization of their chemical compositions using
597 commercially available kits. Total carbohydrate was determined by the Dubois phenol-
598 sulfuric acid method (76) adapted to a 96-well plate assay with the Total Carbohydrate
599 Assay Kit (MAK 104, Sigma-Aldrich), using D-glucose as the standard and absorbance
600 read at a wavelength of 490 nm. Total protein content was determined by the Lowry
601 method (77) adapted to a 96-well plate assay with the Microplate BCA Protein Assay Kit
602 (23252, Thermo Scientific), using bovine serum albumin (BSA) as the standard and
603 absorbance read at OD_{595}. Total eDNA was determined by the Quant-iT™ PicoGreen®
604 dsDNA Assay Kit (P11496, Invitrogen™) adapted to a 96-well plate, using double
605 stranded lambda DNA as the standard and relative fluorescence units (RFU) read with
606 470 nm excitation and 525 nm detection. All readings for chemical composition were
607 performed on a Biotek Synergy H1.

608

609 **Mouse model of CAUTI.** CAUTI studies were carried out as previously described (43).
610 Briefly, the inoculum was prepared by washing overnight cultures of wild-type *P.*
611 *mirabilis* and the Δ*katA* mutant in PBS, adjusting each to an OD_{600} of 0.2 (~2 x 10^8
612 CFU/ml), and diluting 1:100 to achieve an inoculum of 2 x 10^6 CFU/ml. Female CBA/J
613 mice aged 6 to 8 weeks (Jackson Laboratory) were anesthetized with a weight-
614 appropriate dose (0.1 ml for a mouse weighing 20 g) of ketamine-xylazine (100 mg/kg
615 ketamine and 10 mg/kg xylazine) by intraperitoneal (i.p.) injection and inoculated
616 transurethrally with 50 µl of the diluted suspension (1 x 10^5 CFU/mouse). A 4-mm
617 segment of sterile silicone tubing (0.64-mm outside diameter [o.d.], 0.30-mm inside

618 diameter [i.d.]; Braintree Scientific, Inc.) was carefully advanced into the bladder during
619 inoculation and retained for the duration of the study as described previously (45, 78).
620 At both 24 and 96 hours post infection (hpi), urine was collected, the mice were
621 euthanized, and bladders, kidneys, and spleens were harvested into 5-ml Eppendorf
622 tubes containing 1 ml PBS. Tissues were homogenized using a Bullet Blender 5 Gold
623 (Next Advance) and plated using an EddyJet 2 spiral plater (Neutec Group) for
624 determination of CFU using a ProtoCOL 3 automated colony counter (Synbiosis).

625

626 **Mouse model of CAUTI using a pre-colonized catheter.** Biofilms of wild-type *P.*
627 *mirabilis* and the Δ*katA* mutant were formed over a 12 hour period on 4-mm segments
628 of sterile silicone tubing (0.64-mm outside diameter [o.d.], 0.30-mm inside diameter
629 [i.d.]; Braintree Scientific, Inc.) and transferred to PBS to remove non-adherent bacteria,
630 resulting in an inoculum of ~2 x 10^6 CFU/ml of biofilm-associated bacteria. Female
631 CBA/J mice aged 6 to 8 weeks (Jackson Laboratory) were anesthetized as described
632 above, and pre-colonized catheter segments were then carefully advanced into the
633 bladder. At 24 hpi urine was collected, the mice were euthanized, and bladders,
634 kidneys, and spleens were harvested and processed as above.

635

636 **Mouse model of bacteremia.** Bacteremia studies were carried out as previously
637 described (79). Briefly, the inoculum was prepared by washing overnight cultures of
638 wild-type *P. mirabilis* and the Δ*katA* mutant in PBS and diluting in PBS to an OD_{600} of
639 0.1 (1 x 10^8 CFU/ml). Female CBA/J mice aged 6 to 8 weeks (Jackson Laboratory) were

inoculated by tail vein injection of 100 µl (1 x 10^7 CFU/mouse) of a 1:1 mixture of the *P. mirabilis* HI4320 and Δ*katA* mutant suspensions. Mice were euthanized 24 hpi, and organs were harvested into 5 ml Eppendorf tubes containing PBS (1 ml for spleens and kidneys, 2 ml for livers). Tissues were homogenized as above and plated onto plain LB agar (total CFU) and LB with kanamycin (Δ*katA* CFU) for determination of CFUs. A competitive index (CI) was calculated as follows for all samples in which bacterial burden was above the limit of detection:

$$\mathbf{CI} = \frac{\boldsymbol{\Delta katA}\ \mathbf{output/WToutput}}{\mathbf{\Delta katA\ input/WT\ input}}$$

$Log_{10}CI = 0$ indicates that the ratio of the strains in the output is similar to the input, and neither strain had an advantage. Log10CI>0 indicates that Δ*katA* has a competitive advantage over wild-type (WT).

Statistical Analysis. Normalcy was assessed for all data sets by the Shapiro-Wilk and D'Agostino-Pearson normality tests. Significance was assessed using two-way analysis of variance (ANOVA), nonparametric Mann-Whitney test, unpaired t test, one-sample t test, chi-square test, or Wilcoxon signed rank test, as indicated in the figure legends. All P values are two tailed at a 95% confidence interval. All analyses were performed using Prism, version 7.03 (GraphPad Software, San Diego, CA).

Acknowledgments

We would like to thank members of the Department of Microbiology & Immunology in the Jacobs School of Medicine and Biomedical Sciences at the University at Buffalo for helpful comments and critiques. This work was supported by the National Institutes of Health [R00 DK105205 and R01 DK123158 to C.E.A.]. The sponsors were not involved in the study design, methods, data collections, analysis, or preparation of the paper. The content is solely the responsibility of the authors and does not necessarily represent the official views of the funders.

Competing Interests

The authors have no financial or non-financial competing interests to declare.

References

1. Wenner JJ, Rettger LF. 1919. A Systematic Study of the Proteus Group of Bacteria. Journal of bacteriology 4:331-353.

2. Hooton T, Bradley S, Cardenas D, Colgan R, Geerlings S, C Rice J, Saint S, Schaeffer A, Tambyah P, Tenke P, E Nicolle L. 2010. Diagnosis, Prevention, and Treatment of Catheter-Associated Urinary Tract Infection in Adults: 2009 International Clinical Practice Guidelines from the Infectious Diseases Society of America, vol 50.

3. Warren JW. 2001. Catheter-associated urinary tract infections. International Journal of Antimicrobial Agents 17:299-303.

4. Jacobsen SM, Stickler DJ, Mobley HLT, Shirtliff ME. 2008. Complicated catheter-associated urinary tract infections due to Escherichia coli and Proteus mirabilis. Clinical microbiology reviews 21:26-59.

5. Li X, Zhao H, Lockatell CV, Drachenberg CB, Johnson DE, Mobley HLT. 2002. Visualization of Proteus mirabilis within the matrix of urease-induced bladder stones during experimental urinary tract infection. Infection and immunity 70:389-394.

6. Armbruster CE, Mobley HLT, Pearson MM. 2018. Pathogenesis of Proteus mirabilis Infection. EcoSal Plus 8:10.1128/ecosalplus.ESP-0009-2017.

7. Griffith DP MD, Itin C. 1976. Urease. The primary cause of infection-induced urinary stones. Investigative Urology 13:346-50.

8. Lo E, Nicolle L, Classen D, Arias KM, Podgorny K, Anderson DJ, Burstin H, Calfee DP, Coffin SE, Dubberke ER, Fraser V, Gerding DN, Griffin FA, Gross P, Kaye KS, Klompas M, Marschall J, Mermel LA, Pegues DA, Perl TM, Saint S, Salgado CD, Weinstein RA, Wise R, Yokoe DS. 2008. Strategies to Prevent Catheter-Associated

691 Urinary Tract Infections in Acute Care Hospitals. Infection Control & Hospital
692 Epidemiology 29:S41-S50.
693 9. Setia U, Serventi I, Lorenz P. 1984. Bacteremia in a long-term care facility: Spectrum
694 and mortality. Archives of Internal Medicine 144:1633-1635.
695 10. Nicolle L, McIntyre M, Hoban D, Murray D. 1994. Bacteremia in a long term care
696 facility. The Canadian journal of infectious diseases = Journal canadien des maladies
697 infectieuses 5:130-132.
698 11. Mylotte JM, Tayara A, Goodnough S. 2002. Epidemiology of Bloodstream Infection in
699 Nursing Home Residents: Evaluation in a Large Cohort from Multiple Homes. Clinical
700 Infectious Diseases 35:1484-1490.
701 12. Melzer M, Welch C. 2013. Outcomes in UK patients with hospital-acquired bacteraemia
702 and the risk of catheter-associated urinary tract infections. Postgraduate medical journal
703 89:329-334.
704 13. Daniels KR, Lee GC, Frei CR. 2014. Trends in catheter-associated urinary tract
705 infections among a national cohort of hospitalized adults, 2001-2010. American Journal
706 of Infection Control 42:17-22.
707 14. Weiner LM, Webb AK, Limbago B, Dudeck MA, Patel J, Kallen AJ, Edwards JR,
708 Sievert DM. 2016. Antimicrobial-Resistant Pathogens Associated With Healthcare-
709 Associated Infections: Summary of Data Reported to the National Healthcare Safety
710 Network at the Centers for Disease Control and Prevention, 2011-2014. Infection control
711 and hospital epidemiology 37:1288-1301.
712 15. Peterson LR. 2009. Bad Bugs, No Drugs: No ESCAPE Revisited. Clinical Infectious
713 Diseases 49:992-993.

16. Pendleton JN, Gorman SP, Gilmore BF. 2013. Clinical relevance of the ESKAPE pathogens. Expert Review of Anti-infective Therapy 11:297-308.

17. Stewart PS, Costerton JW. 2001. Antibiotic resistance of bacteria in biofilms. Lancet 358:135-8.

18. Macleod SM, Stickler DJ. 2007. Species interactions in mixed-community crystalline biofilms on urinary catheters. Journal of Medical Microbiology 56:1549-1557.

19. Stickler DJ, Morgan SD. 2008. Observations on the development of the crystalline bacterial biofilms that encrust and block Foley catheters. J Hosp Infect 69:350-60.

20. Stickler D, Ganderton L, King J, Nettleton J, Winters C. 1993. Proteus mirabilis biofilms and the encrustation of urethral catheters. Urological Research 21:407-411.

21. Stickler D, Morris N, Moreno MC, Sabbuba N. 1998. Studies on the formation of crystalline bacterial biofilms on urethral catheters. Eur J Clin Microbiol Infect Dis 17:649-52.

22. Roshni Amalaradjou MAV, Kumar. 2013. Role of Bacterial Biofilms in Catheter-Associated Urinary Tract Infections (CAUTI) and Strategies for Their Control. *In* (ed), IntechOpen, doi:10.5772/55200.

23. Muzzi-Bjornson L, Macera L. 2011. Preventing infection in elders with long-term indwelling urinary catheters. J Am Acad Nurse Pract 23:127-34.

24. Walker JNea. 2019. High-resolution imaging reveals microbial biofilms on patient urinary catheters despite antibiotic administration. World Journal of Urology

25. TALSMA SS. 2007. Biofilms on Medical Devices. Home Healthcare Now 25:589-594.

735 26. Wasfi R, Hamed SM, Amer MA, Fahmy LI. 2020. Proteus mirabilis Biofilm:
736 Development and Therapeutic Strategies. Frontiers in cellular and infection microbiology
737 10:414-414.
738 27. Jacobsen SM, Shirtliff ME. 2011. Proteus mirabilis biofilms and catheter-associated
739 urinary tract infections. Virulence 2:460-465.
740 28. Donlan RM. 2001. Biofilm Formation: A Clinically Relevant Microbiological Process.
741 Clinical Infectious Diseases 33:1387-1392.
742 29. Lewandowski Z. 2000. Structure and Function of Biofilms ppp. 1-17, In: Biofilms:
743 Recent Advances in Their Study and Control, LV Evans (ed). Harwood Academic
744 Publishers.
745 30. Donlan RM. 2002. Biofilms: microbial life on surfaces. Emerging infectious diseases
746 8:881-890.
747 31. Stewart PS. 1996. Theoretical aspects of antibiotic diffusion into microbial biofilms.
748 Antimicrobial agents and chemotherapy 40:2517-2522.
749 32. Stewart PS, Raquepas JB. 1995. Implications of reaction-diffusion theory for the
750 disinfection of microbial biofilms by reactive antimicrobial agents. Chemical Engineering
751 Science 50:3099-3104.
752 33. Burmølle M, Webb JS, Rao D, Hansen LH, Sørensen SJ, Kjelleberg S. 2006. Enhanced
753 biofilm formation and increased resistance to antimicrobial agents and bacterial invasion
754 are caused by synergistic interactions in multispecies biofilms. Appl Environ Microbiol
755 72:3916-23.

34. Stewart PS, Roe F, Rayner J, Elkins JG, Lewandowski Z, Ochsner UA, Hassett DJ. 2000. Effect of catalase on hydrogen peroxide penetration into Pseudomonas aeruginosa biofilms. Applied and environmental microbiology 66:836-838.

35. Staerck C, Gastebois A, Vandeputte P, Calenda A, Larcher G, Gillmann L, Papon N, Bouchara J-P, Fleury MJJ. 2017. Microbial antioxidant defense enzymes. Microbial Pathogenesis 110:56-65.

36. Cornelis P, Wei Q, Andrews SC, Vinckx T. 2011. Iron homeostasis and management of oxidative stress response in bacteria. Metallomics 3:540-549.

37. Yeom J, Imlay JA, Park W. 2010. Iron homeostasis affects antibiotic-mediated cell death in Pseudomonas species. J Biol Chem 285:22689-95.

38. Van Acker H, Gielis J, Acke M, Cools F, Cos P, Coenye T. 2016. The Role of Reactive Oxygen Species in Antibiotic-Induced Cell Death in Burkholderia cepacia Complex Bacteria. PloS one 11:e0159837-e0159837.

39. Eason MM, Fan X. 2014. The role and regulation of catalase in respiratory tract opportunistic bacterial pathogens. Microb Pathog 74:50-8.

40. Dariush M-T, Imana SA, Mina KM, Zahra SD, Elmira RZ, Tahmineh EP. 2014. Comparing Inhibitory Effect of Tramadol on Catalase of Pseudomonas aeruginosa and Mouse Liver. Current Enzyme Inhibition 10:53-57.

41. Taylor WI, Achanzar D. 1972. Catalase test as an aid to the identification of Enterobacteriaceae. Applied microbiology 24:58-61.

42. Pearson MM, Yep A, Smith SN, Mobley HLT. 2011. Transcriptome of Proteus mirabilis in the murine urinary tract: virulence and nitrogen assimilation gene expression. Infection and immunity 79:2619-2631.

779 43. Armbruster CE, Forsyth-DeOrnellas V, Johnson AO, Smith SN, Zhao L, Wu W, Mobley
780 HLT. 2017. Genome-wide transposon mutagenesis of Proteus mirabilis: Essential genes,
781 fitness factors for catheter-associated urinary tract infection, and the impact of
782 polymicrobial infection on fitness requirements. PLoS pathogens 13:e1006434-
783 e1006434.
784 44. Armbruster CE, Forsyth VS, Johnson AO, Smith SN, White AN, Brauer AL, Learman
785 BS, Zhao L, Wu W, Anderson MT, Bachman MA, Mobley HLT. 2019. Twin arginine
786 translocation, ammonia incorporation, and polyamine biosynthesis are crucial for Proteus
787 mirabilis fitness during bloodstream infection. PLOS Pathogens 15:e1007653.
788 45. Armbruster CE, Smith SN, Johnson AO, DeOrnellas V, Eaton KA, Yep A, Mody L, Wu
789 W, Mobley HLT. 2017. The Pathogenic Potential of Proteus mirabilis Is Enhanced by
790 Other Uropathogens during Polymicrobial Urinary Tract Infection. Infection and
791 Immunity 85:e00808-16.
792 46. Jesaitis AJ, Franklin MJ, Berglund D, Sasaki M, Lord CI, Bleazard JB, Duffy JE,
793 Beyenal H, Lewandowski Z. 2003. Compromised Host Defense on Pseudomonas
794 aeruginosa Biofilms: Characterization of Neutrophil and Biofilm Interactions. The
795 Journal of Immunology 171:4329.
796 47. Hirschfeld J. 2014. Dynamic interactions of neutrophils and biofilms. Journal of oral
797 microbiology 6:26102-26102.
798 48. Rada B. 2017. Interactions between Neutrophils and Pseudomonas aeruginosa in Cystic
799 Fibrosis. Pathogens 6:10.

800 49. Haraoka M, Hang L, Frendéus B, Godaly G, Burdick M, Strieter R, Svanborg C. 1999.
801 Neutrophil Recruitment and Resistance to Urinary Tract Infection. The Journal of
802 Infectious Diseases 180:1220-1229.
803 50. Guiton PS, Hannan TJ, Ford B, Caparon MG, Hultgren SJ. 2013. Enterococcus faecalis
804 overcomes foreign body-mediated inflammation to establish urinary tract infections.
805 Infection and immunity 81:329-339.
806 51. Hayes BW, Abraham SN. 2016. Innate Immune Responses to Bladder Infection.
807 Microbiology spectrum 4:10.1128/microbiolspec.UTI-0024-2016.
808 52. Wang J-T, Chen P-C, Chang S-C, Shiau Y-R, Wang H-Y, Lai J-F, Huang IW, Tan M-C,
809 Lauderdale T-LY, Hospitals T. 2014. Antimicrobial susceptibilities of Proteus mirabilis:
810 a longitudinal nationwide study from the Taiwan surveillance of antimicrobial resistance
811 (TSAR) program. BMC infectious diseases 14:486-486.
812 53. Kanayama A, Kobayashi I, Shibuya K. 2015. Distribution and antimicrobial
813 susceptibility profile of extended-spectrum β-lactamase-producing Proteus mirabilis
814 strains recently isolated in Japan. Int J Antimicrob Agents 45:113-8.
815 54. Girlich D, Bonnin RA, Dortet L, Naas T. 2020. Genetics of Acquired Antibiotic
816 Resistance Genes in Proteus spp. Front Microbiol 11:256.
817 55. Adamus-Bialek W, Zajac E, Parniewski P, Kaca W. 2013. Comparison of antibiotic
818 resistance patterns in collections of Escherichia coli and Proteus mirabilis uropathogenic
819 strains. Mol Biol Rep 40:3429-35.
820 56. Ahn JY, Ann HW, Jeon Y, Ahn MY, Oh DH, Kim YC, Kim EJ, Song JE, Jung IY, Kim
821 MH, Jeong W, Ku NS, Jeong SJ, Choi JY, Yong D, Song YG, Kim JM. 2017. The impact

of production of extended-spectrum β-lactamases on the 28-day mortality rate of patients with Proteus mirabilis bacteremia in Korea. BMC infectious diseases 17:327-327.

57. Endimiani A, Luzzaro F, Brigante G, Perilli M, Lombardi G, Amicosante G, Rossolini GM, Toniolo A. 2005. Proteus mirabilis bloodstream infections: risk factors and treatment outcome related to the expression of extended-spectrum beta-lactamases. Antimicrobial agents and chemotherapy 49:2598-2605.

58. Tumbarello M, Trecarichi EM, Fiori B, Losito AR, D'Inzeo T, Campana L, Ruggeri A, Di Meco E, Liberto E, Fadda G, Cauda R, Spanu T. 2012. Multidrug-resistant Proteus mirabilis bloodstream infections: risk factors and outcomes. Antimicrobial agents and chemotherapy 56:3224-3231.

59. Luzzaro F, Ortisi G, Larosa M, Drago M, Brigante G, Gesu G. 2011. Prevalence and epidemiology of microbial pathogens causing bloodstream infections: results of the OASIS multicenter study. Diagn Microbiol Infect Dis 69:363-9.

60. Korytny A, Riesenberg K, Saidel-Odes L, Schlaeffer F, Borer A. 2016. Bloodstream infections caused by multi-drug resistant Proteus mirabilis: Epidemiology, risk factors and impact of multi-drug resistance. Infect Dis (Lond) 48:428-31.

61. Aquilini E, Azevedo J, Jimenez N, Bouamama L, Tomás JM, Regué M. 2010. Functional identification of the Proteus mirabilis core lipopolysaccharide biosynthesis genes. J Bacteriol 192:4413-24.

62. Vinogradov E. 2011. Structure of the core part of the lipopolysaccharide from Proteus mirabilis genomic strain HI4320. Biochemistry (Mosc) 76:803-7.

843 63. Elkins JG, Hassett DJ, Stewart PS, Schweizer HP, McDermott TR. 1999. Protective role
844 of catalase in Pseudomonas aeruginosa biofilm resistance to hydrogen peroxide. Applied
845 and environmental microbiology 65:4594-4600.
846 64. Moradali MF, Ghods S, Rehm BHA. 2017. Pseudomonas aeruginosa Lifestyle: A
847 Paradigm for Adaptation, Survival, and Persistence. Frontiers in Cellular and Infection
848 Microbiology 7.
849 65. Matsukawa M, Greenberg EP. 2004. Putative exopolysaccharide synthesis genes
850 influence Pseudomonas aeruginosa biofilm development. J Bacteriol 186:4449-56.
851 66. Vestby LK, Grønseth T, Simm R, Nesse LL. 2020. Bacterial Biofilm and its Role in the
852 Pathogenesis of Disease. Antibiotics (Basel, Switzerland) 9:59.
853 67. Marks LR, Davidson BA, Knight PR, Hakansson AP. 2013. Interkingdom signaling
854 induces Streptococcus pneumoniae biofilm dispersion and transition from asymptomatic
855 colonization to disease. mBio 4:e00438-13.
856 68. Spitznagel JK, Shafer WM. 1985. Neutrophil Killing of Bacteria by Oxygen-Independent
857 Mechanisms: A Historical Summary. Reviews of Infectious Diseases 7:398-403.
858 69. Standish AJ, Weiser JN. 2009. Human Neutrophils Kill Streptococcus pneumoniae via
859 Serine Proteases. The Journal of Immunology 183:2602-2609.
860 70. Segal AW. 2005. How neutrophils kill microbes. Annu Rev Immunol 23:197-223.
861 71. Slauch JM. 2011. How does the oxidative burst of macrophages kill bacteria? Still an
862 open question. Mol Microbiol 80:580-3.
863 72. Iles KE, Forman HJ. 2002. Macrophage signaling and respiratory burst. Immunol Res
864 26:95-105.

865 73. Mobley HL, Warren JW. 1987. Urease-positive bacteriuria and obstruction of long-term
866 urinary catheters. Journal of clinical microbiology 25:2216-2217.
867 74. Pearson MM, Mobley HLT. 2007. The type III secretion system of Proteus mirabilis
868 HI4320 does not contribute to virulence in the mouse model of ascending urinary tract
869 infection. Journal of Medical Microbiology 56:1277-1283.
870 75. Bales PM, Renke EM, May SL, Shen Y, Nelson DC. 2013. Purification and
871 Characterization of Biofilm-Associated EPS Exopolysaccharides from ESKAPE
872 Organisms and Other Pathogens. PLOS ONE 8:e67950.
873 76. Dubois M, Gilles K, Hamilton JK, Rebers PA, Smith F. 1951. A Colorimetric Method for
874 the Determination of Sugars. Nature 168:167-167.
875 77. Lowry OH, Rosebrough NJ, Farr AL, Randall RJ. 1951. Protein measurement with the
876 Folin phenol reagent. The Journal of biological chemistry 193:265-275.
877 78. Guiton PS, Hung CS, Hancock LE, Caparon MG, Hultgren SJ. 2010. Enterococcal
878 Biofilm Formation and Virulence in an Optimized Murine Model of Foreign Body-
879 Associated Urinary Tract Infections. Infection and Immunity 78:4166.
880 79. Smith SN, Hagan EC, Lane MC, Mobley HLT. 2010. Dissemination and Systemic
881 Colonization of Uropathogenic <span class="named-content genus-
882 species" id="named-content-1">Escherichia coli in a
883 Murine Model of Bacteremia. mBio 1:e00262-10.

884

885

886

CAUTI Disease Severity	24h Standard CAUTI[(A)]			96h Standard CAUTI[(B)]			24h Pre-col CAUTI[(C)]			24h Standard CAUTI vs 24h Pre-col CAUTI (WT comparison)[(D)]		
	WT	Δ*katA*	*P* value	WT	Δ*katA*	*P* value	WT	Δ*katA*	*P* value	CAUTI	Pre-col	*P* value
Bladder hematoma and/or blood in urine	0/12	0/12	-	0/14	0/13	-	8/11	0/11	0.0004	0/12	8/11	0.0003
Kidney hematoma	0/12	0/12	-	0/14	0/13	-	2/11	0/11	0.1380	0/12	2/11	0.1221
Kidney color change and/or mottling	0/12	0/12	-	3/14	3/13	-	8/11	5/11	0.1930	0/12	8/11	0.0003
Kidney stone	0/12	0/12	-	5/14	2/13	0.2280	4/11	0/11	0.0270	0/12	4/11	0.0215
Any abnormality	0/12	0/12	-	7/14	4/13	0.3090	9/11	5/11	0.0760	0/12	9/11	0.0001

Table 1: *CAUTI disease severity.* All mice were assessed for the following parameters at the time of urine collection and euthanasia: bladder hematoma and/or blood in urine, kidney hematoma, kidney color change and/or mottling, and kidney stones. “Any abnormality” indicates whether at least one of these parameters was detected in a mouse. Data represent the number of mice positive for the above parameters out of the total mice infected for each strain during (A) 24h and (B) 96h standard CAUTI model, (C) 24h pre-colonized CAUTI model, and (D) a comparison of mice infected with WT between the two models at 24h. P values were determined by Chi-square test.

Figure Legends

Figure 1: *Characterization of a P. mirabilis* Δ*katA mutant*. The *ΔkatA* mutant was assessed for catalase activity (A), growth in LB (B), urease activity (C), swimming motility (D), and swarming motility (E) in comparison to wild-type *P. mirabilis*. (A) An SDS/peroxide foam height assay was conducted to provide phenotypic validation of successful generation of a *P. mirabilis* Δ*katA* mutant and plasmid generated Δ*katA*+ complemented strain. (B) Bacterial growth in LB at 37°C was assessed by measurement of OD_{600} at hourly intervals for 18 hours. Error bars represent mean ± standard deviation (SD) of 6 independent experiments with 6 technical replicates each (representative graph shown). No significant differences in growth were determined by two-way ANOVA with Dunnett's test for multiple comparisons. (C) Urease activity in human urine was assessed by measurement of phenol red color change (OD_{562}) at 5-minute intervals for 80 minutes, and a *P. mirabilis* Δ*ureF* mutant was included as negative control. Error bars represent mean ± SD of 2 independent experiments with 6 technical replicates each. No significant differences between WT and Δ*katA* were identified by two-way ANOVA. (D and E) Bacteria were cultured in LB broth overnight and stab inoculated into motility agar (D) or inoculated onto the surface of swarm agar plates (E). Motility diameter was measured in millimeters after 16 hours of incubation at 30°C (D) or 37°C (E). R1-3 indicate individual swarm ring diameters. Error bars represent mean ± SD for 3 independent experiments with at least 2 replicates each. No significant differences in motility diameter were determined by Student's t test (D) or two-way ANOVA (E).

Figure 2: *Disruption of katA increases sensitivity to hydrogen peroxide and steady-state ROS levels*. (A-E) Growth at 37°C was assessed by measurement of OD_{600} at hourly intervals for 18 hours for wild-type (WT, black), Δ*katA* mutant (light gray), and plasmid generated Δ*katA*+ complemented strain (dark gray) in (A) plain LB or in the presence of increasing concentrations of hydrogen peroxide (H_2O_2) as follows: (B) 0.0015% v/v (~2 mM), (C) 0.0025% v/v (~3 mM), (D) 0.1% v/v (~109 mM), and (E) 0.3% v/v (~326 mM). Error bars represent mean ± standard deviation (SD) of 3 independent experiments with 6 technical replicates each. (F) Peroxide standard curve for measurement of reactive oxygen species in bacterial cultures. (G) H_2O_2 concentrations present in cultures of WT (dark gray) and Δ*katA* (white) after a 4-hour incubation in LB broth. Individual data points represent 3 independent experiments with technical duplicates, and the WT and Δ*katA* values from each experiment are connected with a black line. (H) Average fold change in *ΔkatA* H_2O_2 levels compared to WT. * $P<0.05$ by one-sample t test.

Figure 3: Δ*katA exhibits a defect in biofilm development.* (A,B) Biofilms of WT (gray), WT+ (+bovine catalase, gray stripes), *ΔkatA* (white), and *ΔkatA+* (+ bovine catalase, light gray) were formed over a timecourse of 20 h in (A) LB or (B) pooled human urine. Biofilm biomass was assessed at 2, 4, 6, 12, and 20 h via crystal violet staining and detected by OD_{570}. (C, D) Biofilms of WT (gray), WT + 0.1% v/v (~109 mM) H_2O_2 (gray dots), and *ΔkatA* (white) were formed over a timecourse of 20 h in (C) LB or (D) pooled human urine. (A-D) Error bars represent mean and SD of 3 independent

experiments with 3 replicates each. *P<0.05, ** P<0.01, ***P<.001 by two-way ANOVA with Sidak's test for multiple comparisons.

Figure 4: Δ*katA* exhibits a defect in biofilm EPS production. (A-D) Representative SEM images of 20 h biofilms formed by (A) WT, (B) Δ*katA*, (C) WT+ bovine catalase, and (D) Δ*katA*+ bovine catalase. (E-G) WT (black circles) and Δ*katA* (white circles) were incubated for 20 h with aeration or stationary to generate planktonic suspensions (PS) and biofilm (BS) suspensions. EPS was further extracted from the biofilm suspension to generate a cellular fraction (CF) and EPS fraction (EF) for measurement of eDNA (E), protein (F), and carbohydrate (G). Box and whisker plots display the combined data from 3 independent experiments with 3 technical replicates each. ***P<.001 by two-way ANOVA with Sidak's test for multiple comparisons.

Figure 5: Δ*katA* biofilms exhibit increased antibiotic susceptibility. (A-C) Growth at 37°C was assessed by measurement of OD_{600} at hourly intervals for 18 hours for WT (black symbols) and *ΔkatA* (white symbols) in the presence of increasing concentrations (µg/ml) of (A) ampicillin, (B) ceftriaxone, or (C) ciprofloxacin. Error bars represent mean ± standard deviation (SD) for 6 technical replicates, and graphs are representative of at least 3 independent experiments. Data were analyzed by two-way ANOVA with Tukey's test for multiple comparisons. (D-I) Biofilms were established by WT and *ΔkatA* for 20 h (D-F) or 4 h (G-I), followed by treatment with increasing concentrations of ampicillin (D and G), ceftriaxone (E and H), or ciprofloxacin (F and I) for an additional 20 h period. Each black (WT), white (Δ*katA*), and light gray (katA+ bovine catalase) circle represents

963 the CFU/ml recovered from an individual biofilm, and box and whisker plots display
964 combined results from at least 3 independent experiments with at least 3 technical
965 replicates each. * P<0.05 , ** P<0.01, ***P<.001 by two-way ANOVA with Sidak's test
966 for multiple comparisons.
967
968 **Figure 6: *ΔkatA exhibits a biofilm biomass defect on silicone catheters.*** (A)
969 Representative images of crystal violet-stained 15 mm silicone Foley catheter segments
970 after 20 h incubation with WT, Δ*katA*, Δ*katA*+ (bovine catalase), or plain LB (blank). (B)
971 Biomass of 20 h WT (gray), *ΔkatA* (white), ΔkatA+ (bovine catalase, light gray) catheter
972 biofilms as assessed by crystal violet staining at OD_{570}. Error bars represent mean and
973 standard deviation (SD) of at least 3 independent experiments with at least 3 technical
974 replicates each. ** P<0.01, ***P<.001 by one-way ANOVA with Tukey's test for multiple
975 comparisons.
976
977 **Figure 7: *katA contributes to P. mirabilis CAUTI and bacteremia.*** (A-B) Female
978 CBA/J mice were transurethrally inoculated with 50 µl of a bacterial suspension
979 containing ~2 x 10^6 CFU/ml of either WT or Δ*katA*, and a 4-mm segment of silicone
980 catheter tubing was advanced into the bladder during inoculation. Mice were euthanized
981 at (A) 24 and (B) 96 h post inoculation (hpi) for determination of bacterial CFUs in the
982 urine, bladder, kidneys, or spleen. Each black (WT) and white (Δ*katA*) circle represents
983 the log10 CFU per milliliter of urine or gram of tissue from an individual mouse, and the
984 dashed line indicates the limit of detection. * P < 0.05, ** P<0.01 by nonparametric
985 Mann-Whitney test. (C) Female CBA/J mice were transurethrally inoculated via insertion

of a 4-mm segment of silicone catheter tubing that had been pre-colonized by either WT or Δ*katA* for 12 h to establish a biofilm (~2 x 10^6 CFU/ml). Mice were euthanized at 24 hpi for analysis of CFUs as above. (D-E) Female CBA/J mice were inoculated via tail vein injection of 100 µl of a bacterial suspension containing 1x10^8 CFU/ml of a 1:1 mixture of wild-type *P. mirabilis* and the Δ*katA* mutant. Mice were euthanized at 24 hpi for determination of bacterial CFUs in the spleen, liver and kidneys. (D) Each black (WT) and white (Δ*katA*) circle connected with a solid line represents the log10 CFU per gram of tissue from an individual mouse. (E) A competitive index (CI) was calculated for the Δ*katA* mutant on a per-mouse basis for the spleen, liver, and kidneys from the ratio of mutant to wild-type recovered from the organ divided by the ratio of mutant to wild-type in the inoculum. Each data point represents the Log10 CI from an individual mouse. Solid lines represent the median, dashed line indicates a competitive index of 1, or a 1:1 ratio of mutant to wild-type. *P < 0.05 by Wilcoxon signed rank test.

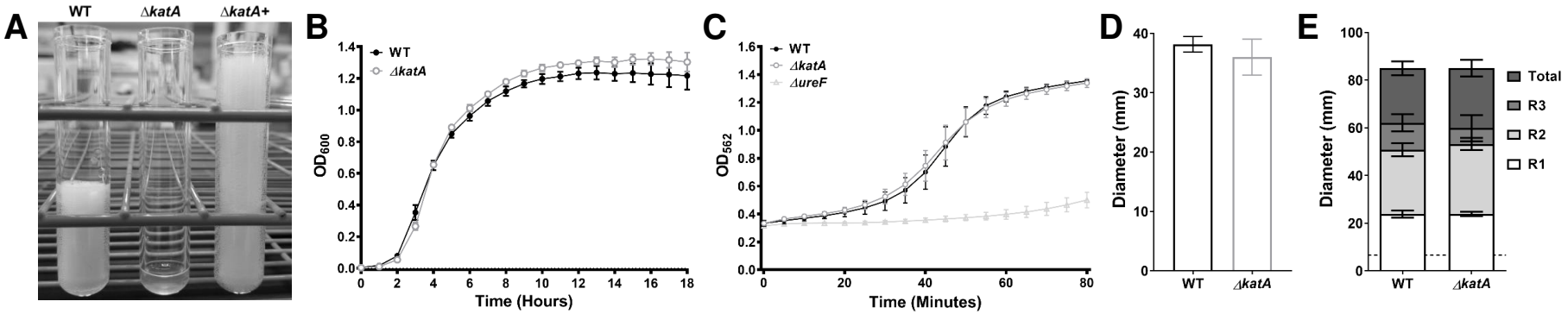

Figure 1: ***Characterization of a P. mirabilis ΔkatA mutant.*** The Δ*katA* mutant was assessed for catalase activity (A), growth in LB (B), urease activity (C), swimming motility (D), and swarming motility (E) in comparison to wild-type *P. mirabilis.* (A) An SDS/peroxide foam height assay was conducted to provide phenotypic validation of successful generation of a *P. mirabilis* Δ*katA* mutant and plasmid generated Δ*katA+* complemented strain. (B) Bacterial growth in LB at 37°C was assessed by measurement of OD_{600} at hourly intervals for 18 hours. Error bars represent mean ± standard deviation (SD) of 6 independent experiments with 6 technical replicates each (representative graph shown). No significant differences in growth were determined by two-way ANOVA with Dunnett's test for multiple comparisons. (C) Urease activity in human urine was assessed by measurement of phenol red color change (OD_{562}) at 5-minute intervals for 80 minutes, and a *P. mirabilis* Δ*ureF* mutant was included as negative control. Error bars represent mean ± SD of 2 independent experiments with 6 technical replicates each. No significant differences between WT and Δ*katA* were identified by two-way ANOVA. (D and E) Bacteria were cultured in LB broth overnight and stab inoculated into motility agar (D) or inoculated onto the surface of swarm agar plates (E). Motility diameter was measured in millimeters after 16 hours of incubation at 30°C (D) or 37°C (E). R1-3 indicate individual swarm ring diameters. Error bars represent mean ± SD for 3 independent experiments with at least 2 replicates each. No significant differences in motility diameter were determined by Student's t test (D) or two-way ANOVA (E).

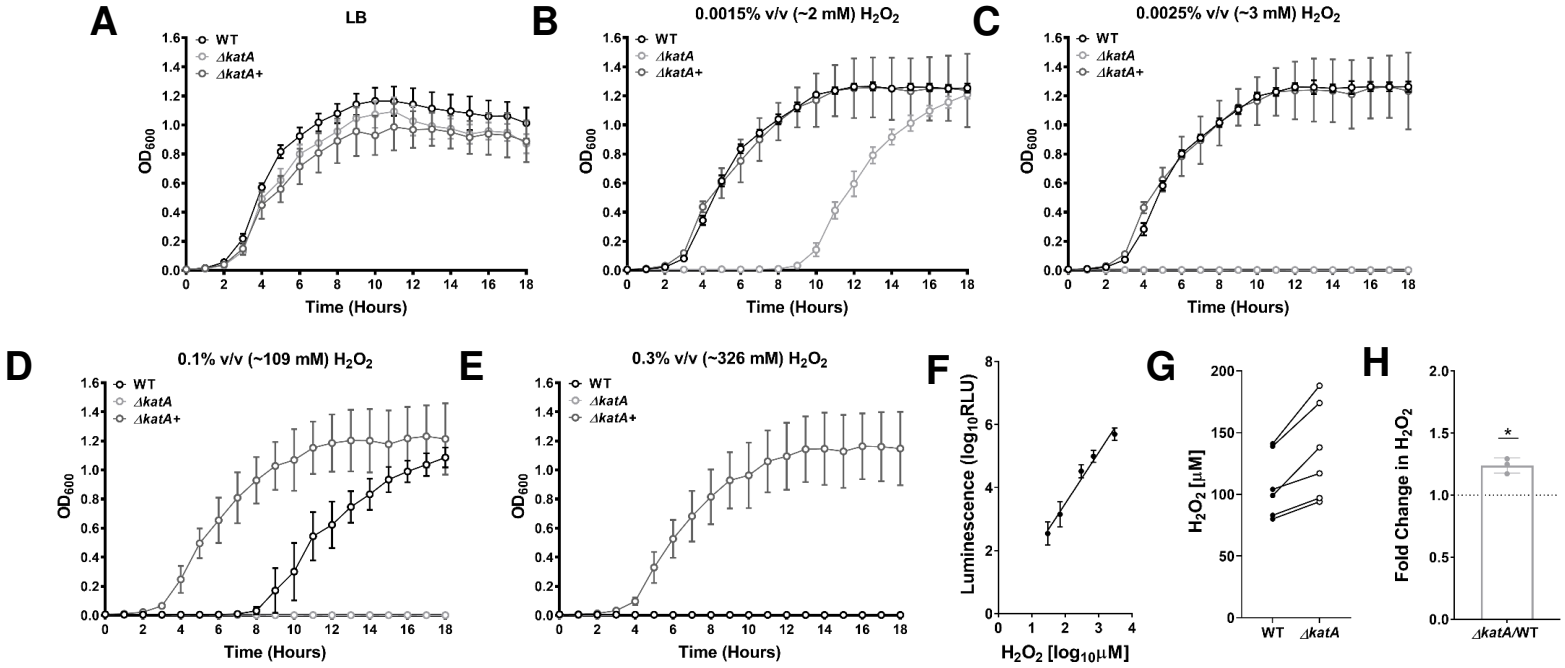

Figure 2: ***Disruption of katA increases sensitivity to hydrogen peroxide and steady-state ROS levels.*** (A-E) Growth at 37°C was assessed by measurement of OD_{600} at hourly intervals for 18 hours for wild-type (WT, black), Δ*katA* mutant (light gray), and plasmid generated Δ*katA+* complemented strain (dark gray) in (A) plain LB or in the presence of increasing concentrations of hydrogen peroxide (H_2O_2) as follows: (B) 0.0015% v/v (~2 mM), (C) 0.0025% v/v (~3 mM), (D) 0.1% v/v (~109 mM), and (E) 0.3% v/v (~326 mM). Error bars represent mean ± standard deviation (SD) of 3 independent experiments with 6 technical replicates each. (F) Peroxide standard curve for measurement of reactive oxygen species in bacterial cultures. (G) H_2O_2 concentrations present in cultures of WT (dark gray) and Δ*katA* (white) after a 4-hour incubation in LB broth. Individual data points represent 3 independent experiments with technical duplicates, and the WT and Δ*katA* values from each experiment are connected with a black line. (H) Average fold change in Δ*katA* H_2O_2 levels compared to WT. * P<0.05 by one-sample t test.

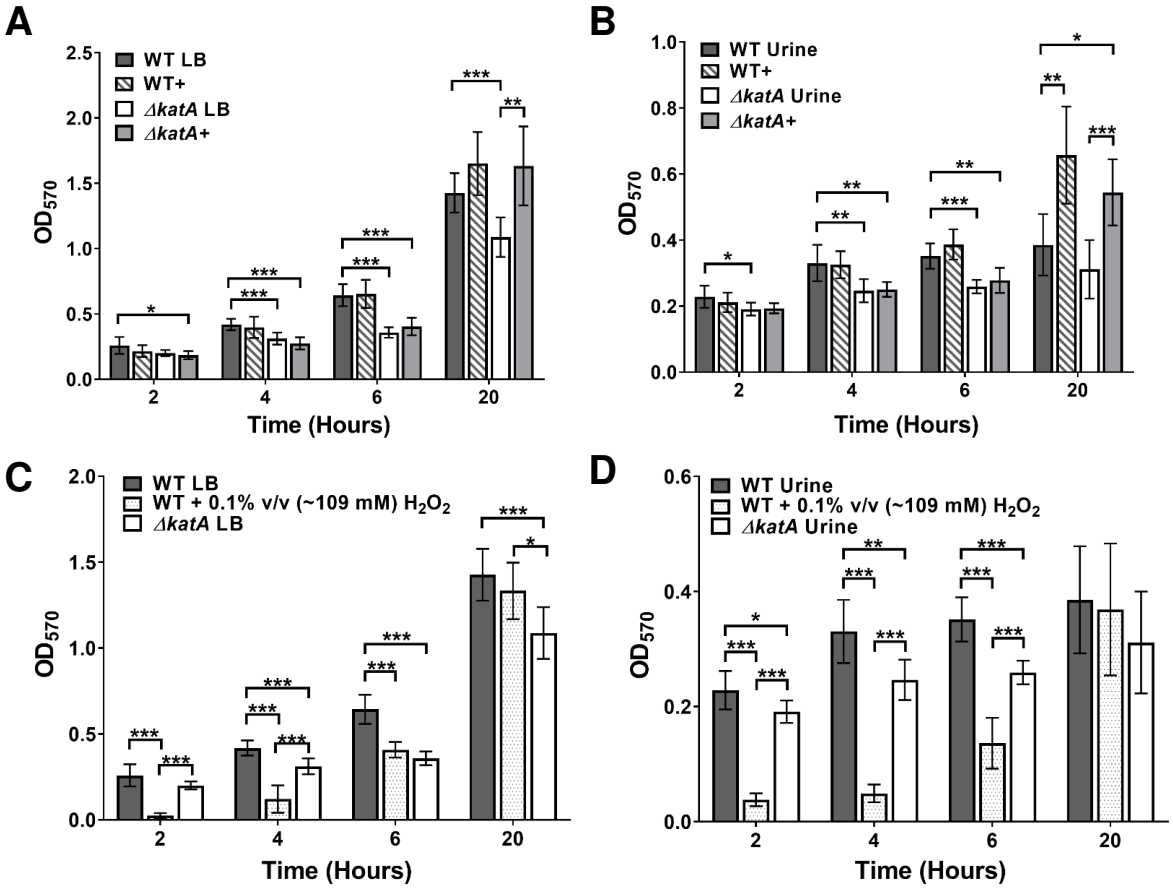

Figure 3: ***ΔkatA exhibits a defect in biofilm development.*** (A,B) Biofilms of WT (gray), WT+ (+bovine catalase, gray stripes), *ΔkatA* (white), and *ΔkatA+* (+ bovine catalase, light gray) were formed over a timecourse of 20 h in (A) LB or (B) pooled human urine. Biofilm biomass was assessed at 2, 4, 6, 12, and 20 h via crystal violet staining and detected by OD_{570}. (C, D) Biofilms of WT (gray), WT + 0.1% v/v (~109 mM) H_2O_2 (gray dots), and *ΔkatA* (white) were formed over a timecourse of 20 h in (C) LB or (D) pooled human urine. (A-D) Error bars represent mean and SD of 3 independent experiments with 3 replicates each. *P<0.05, ** P<0.01, ***P<.001 by two-way ANOVA with Sidak's test for multiple comparisons.

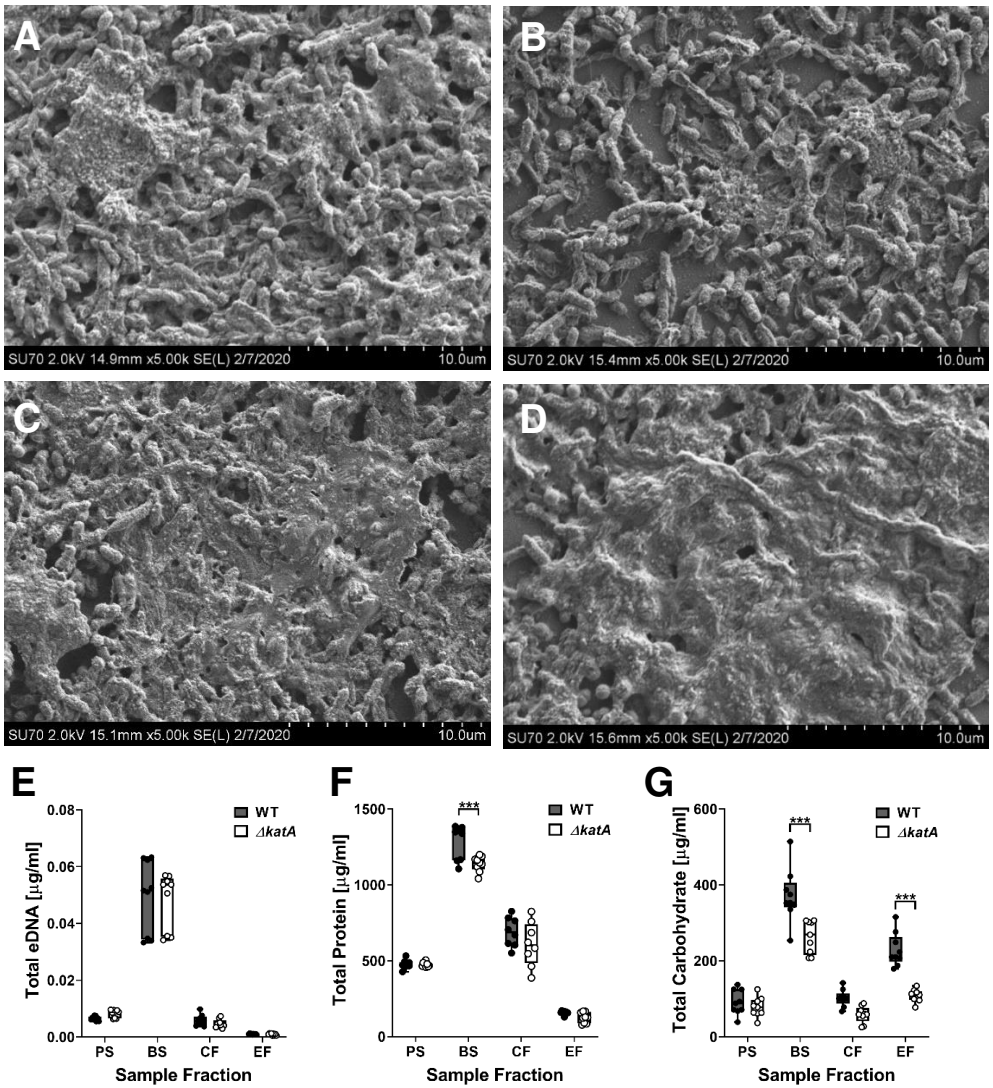

Figure 4: (A-D) Representative SEM images of 20 h biofilms formed by (A) WT, (B) Δ*katA*, (C) WT+ bovine catalase, and (D) Δ*katA+* bovine catalase. (E-G) WT (black circles) and Δ*katA* (white circles) were incubated for 20 h with aeration or stationary to generate planktonic suspensions (PS) and biofilm (BS) suspensions. EPS was further extracted from the biofilm suspension to generate a cellular fraction (CF) and EPS fraction (EF) for measurement of eDNA (E), protein (F), and carbohydrate (G). Box and whisker plots display the combined data from 3 independent experiments with 3 technical replicates each. ***P<.001 by two-way ANOVA with Sidak's test for multiple comparisons .

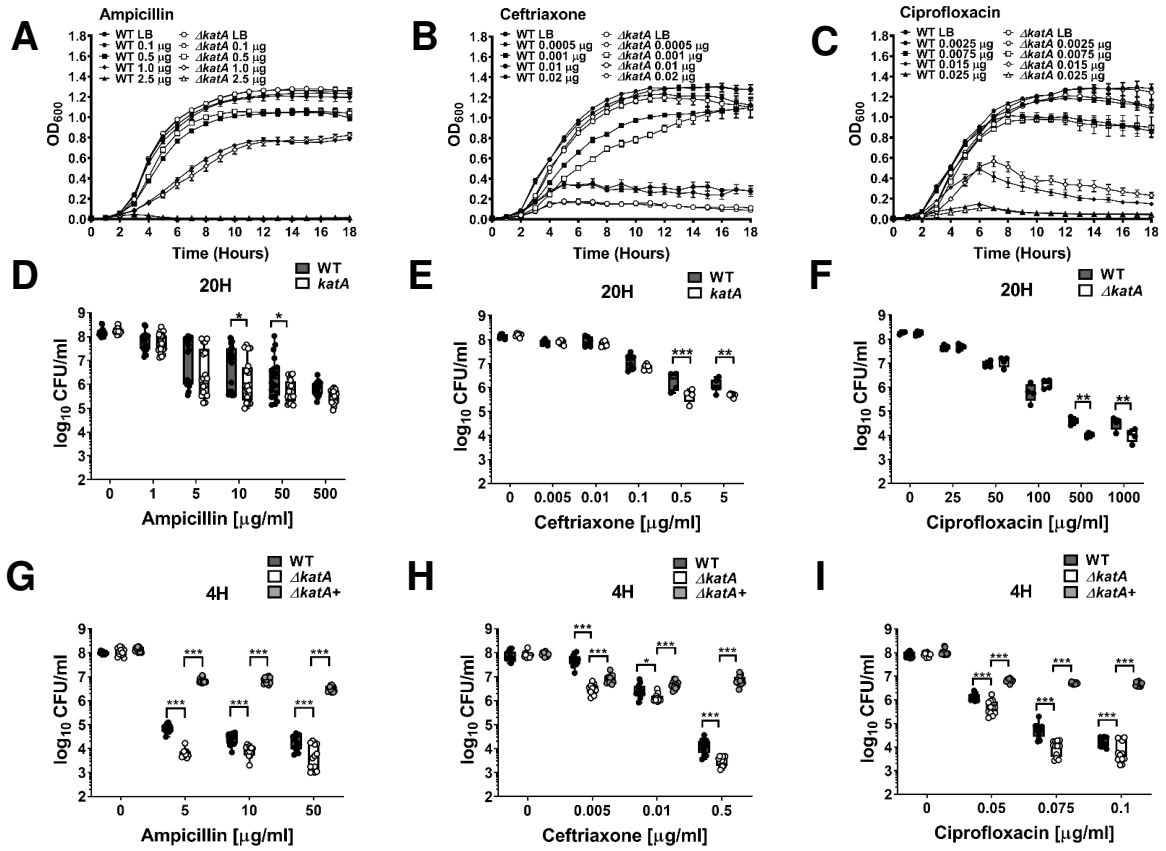

Figure 5: Δ*katA* biofilms exhibit increased antibiotic susceptibility. (A-C) Growth at 37°C was assessed by measurement of OD_{600} at hourly intervals for 18 hours for WT (black symbols) and *ΔkatA* (white symbols) in the presence of increasing concentrations (μg/ml) of (A) ampicillin, (B) ceftriaxone, or (C) ciprofloxacin. Error bars represent mean ± standard deviation (SD) for 6 technical replicates, and graphs are representative of at least 3 independent experiments. Data were analyzed by two-way ANOVA with Tukey's test for multiple comparisons. (D-I) Biofilms were established by WT and *ΔkatA* for 20 h (D-F) or 4 h (G-I), followed by treatment with increasing concentrations of ampicillin (D and G), ceftriaxone (E and H), or ciprofloxacin (F and I) for an additional 20 h period. Each black (WT), white (Δ*katA*), and light gray (katA+ bovine catalase) circle represents the CFU/ml recovered from an individual biofilm, and box and whisker plots display combined results from at least 3 independent experiments with at least 3 technical replicates each. * P<0.05 , ** P<0.01, ***P<.001 by two-way ANOVA with Sidak's test for multiple comparisons .

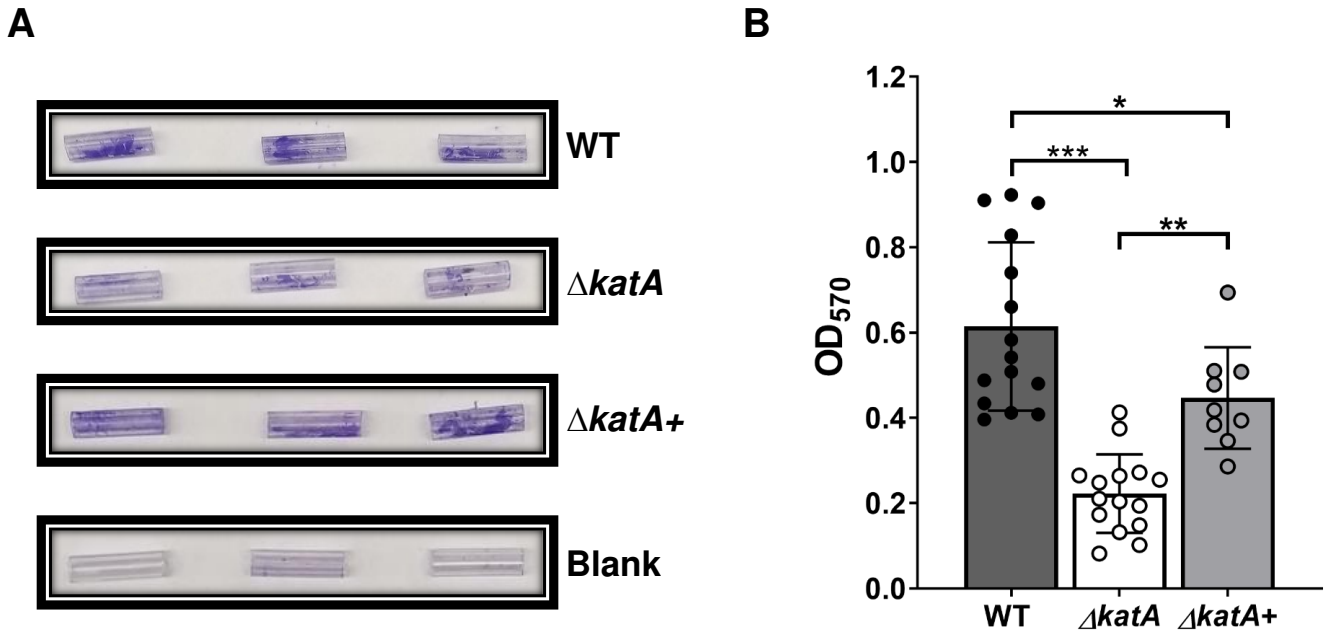

Figure 6: ***ΔkatA exhibits a biofilm biomass defect on silicone catheters.*** (A) Representative images of crystal violet-stained 15mm silicone Foley catheter segments after 20 h incubation with WT, Δ*katA*, Δ*katA+* (bovine catalase), or plain LB (blank). (B) Biomass of 20 h WT (gray), *ΔkatA* (white), ΔkatA+ (bovine catalase, light gray) catheter biofilms as assessed by crystal violet staining at OD_{570}. Error bars represent mean and standard deviation (SD) of at least 3 independent experiments with at least 3 technical replicates each. ** P<0.01, ***P<.001 by one-way ANOVA with Tukey's test for multiple comparisons

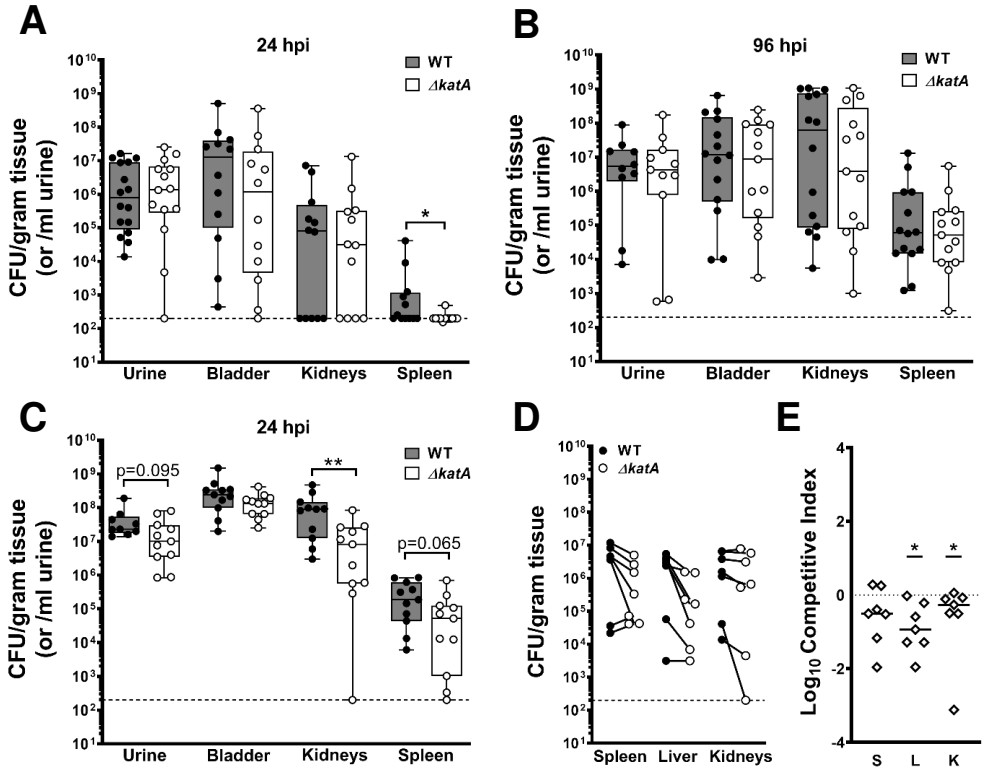

Figure 7: ***katA contributes to P. mirabilis CAUTI and bacteremia.*** (A-B) Female CBA/J mice were transurethrally inoculated with 50 µl of a bacterial suspension containing ~2 x 10^6 CFU/ml of either WT or Δ*katA*, and a 4-mm segment of silicone catheter tubing was advanced into the bladder during inoculation. Mice were euthanized at (A) 24 and (B) 96 h post inoculation (hpi) for determination of bacterial CFUs in the urine, bladder, kidneys, or spleen. Each black (WT) and white (Δ*katA*) circle represents the log10 CFU per milliliter of urine or gram of tissue from an individual mouse, and the dashed line indicates the limit of detection. * $P < 0.05$, ** $P<0.01$ by nonparametric Mann-Whitney test. (C) Female CBA/J mice were transurethrally inoculated via insertion of a 4-mm segment of silicone catheter tubing that had been pre-colonized by either WT or Δ*katA* for 12 h to establish a biofilm (~2 x 10^6 CFU/ml). Mice were euthanized at 24 hpi for analysis of CFUs as above. (D-E) Female CBA/J mice were inoculated via tail vein injection of 100 µl of a bacterial suspension containing 1x10^8 CFU/ml of a 1:1 mixture of wild-type *P. mirabilis* and the Δ*katA* mutant. Mice were euthanized at 24 hpi for determination of bacterial CFUs in the spleen, liver and kidneys. (D) Each black (WT) and white (Δ*katA*) circle connected with a solid line represents the log10 CFU per gram of tissue from an individual mouse. (E) A competitive index (CI) was calculated for the Δ*katA* mutant on a per-mouse basis for the spleen, liver, and kidneys from the ratio of mutant to wild-type recovered from the organ divided by the ratio of mutant to wild-type in the inoculum. Each data point represents the Log10 CI from an individual mouse. Solid lines represent the median, dashed line indicates a competitive index of 1, or a 1:1 ratio of mutant to wild-type. *$P < 0.05$ by Wilcoxon signed rank test.